Geophys. J. Int. (2010) **181,** 81–98 doi: 10.1111/j.1365-246X.2010.04522.x

Post-seismic and interseismic fault creep I: model description

E. A. Hetland,[1]* M. Simons[1] and E. M. Dunham[2]†

[1]*Seismological Laboratory, California Institute of Technology, Pasadena, CA, USA. E-mail: ehetland@alum.mit.edu*
[2]*Department of Earth and Panetary Sciences, Harvard University, Cambridge, MA, USA*

Accepted 2010 January 13. Received 2009 October 8; in original form 2009 March 22

SUMMARY

We present a model of localized, aseismic fault creep during the full interseismic period, including both transient and steady fault creep, in response to a sequence of imposed coseismic slip events and tectonic loading. We consider the behaviour of models with linear viscous, non-linear viscous, rate-dependent friction, and rate- and state-dependent friction fault rheologies. Both the transient post-seismic creep and the pattern of steady interseismic creep rates surrounding asperities depend on recent coseismic slip and fault rheologies. In these models, post-seismic fault creep is manifest as pulses of elevated creep rates that propagate from the coseismic slip, these pulses feature sharper fronts and are longer lived in models with rate-state friction compared to other models. With small characteristic slip distances in rate-state friction models, interseismic creep is similar to that in models with rate-dependent friction faults, except for the earliest periods of post-seismic creep. Our model can be used to constrain fault rheologies from geodetic observations in cases where the coseismic slip history is relatively well known. When only considering surface deformation over a short period of time, there are strong trade-offs between fault rheology and the details of the imposed coseismic slip. Geodetic observations over longer times following an earthquake will reduce these trade-offs, while simultaneous modelling of interseismic and post-seismic observations provide the strongest constraints on fault rheologies.

Key words: Seismic cycle; Rheology and friction of fault zones; Dynamics and mechanics of faulting.

1 INTRODUCTION

Geodetic observations in seismogenic plate boundaries record deformation during various phases in the seismic cycle, including coseismic, post-seismic and interseismic deformation. Ignoring the details of the earthquake process, coseismic deformation is manifest in geodetic observations as instantaneous offsets. On the other hand, geodetic observations of post-seismic deformation record a rich transient mechanical response of the lithosphere, while the deformation observed during the later interseismic period is nearly steady in time. The term 'interseismic' often refers to the secular, steady deformation recorded late in a seismic cycle. Here we consider both transient and secular deformation to be interseismic, and we use 'interseismic period' to refer to the entire period between earthquakes. We use post-seismic to specifically refer to transient deformation immediately following earthquakes.

We develop a model of localized, aseismic fault creep during the full interseismic period, including both transient and steady localized fault creep. (Throughout this paper we use 'creep' to refer to aseismic fault slip.) We do not solve for phenomena associated with the earthquake process (nucleation, seismic slip propagation, etc.), rather our model only includes creep in response to repeated earthquakes on the fault and loading of the fault. We present this more limited model in order to explore interseismic creep following known earthquakes, and to eventually be used to constrain fault zone properties from geodetic observations.

Coseismic, post-seismic, and interseismic deformation are intricately linked, with post-seismic deformation caused by coseismic stress changes, and interseismic deformation the result of transient deformation due to all previous earthquakes plus tectonic loading (e.g. Hetland & Hager 2006b). Ideally a comprehensive model of deformation throughout the entire earthquake cycle would include all three of these phases of deformation (e.g. Rice 1993; Lapusta *et al.* 2000; Liu & Rice 2005; Hori 2006; Kato 2008). However, these models contain so much inherent physical complexity that it is difficult to tie specific calculations of interseismic deformation to known earthquake sequences.

A truly comprehensive model of seismic cycle deformation would also include both off-fault (e.g. Jónsson *et al.* 2003; Freed & Bürgmann 2004; Hetland & Hager 2005; Savage *et al.* 2005) and fault zone rheologies (e.g. Marone *et al.* 1991; Rice 1993; Montési 2004a). However, there are many instances where only

*Now at: Department of Geological Sciences, 2534 CC Little Bldg., University of Michigan, Ann Arbor, MI 48109, USA.
†Now at: Department of Geophysics, Stanford University, Palo Alto, CA, USA.

© 2010 The Authors
Journal compilation © 2010 RAS

localized fault creep is sufficient to explain available observations. For example, geodetic observations of both transient post-seismic and steady interseismic observations at Parkfield, CA, can be explained by models with only fault creep (e.g. Marone *et al.* 1991; Murray *et al.* 2001; Johnson *et al.* 2006; Freed 2007). Following larger continental earthquakes, a single mechanical response of the lithosphere is often insufficient to fully describe either post-seismic (e.g. Fialko 2004; Freed *et al.* 2006; Hearn *et al.* 2009) or interseismic (e.g. Johnson & Segall 2004) deformation, although the earliest post-seismic deformation can frequently be described by creep of the fault (e.g. Hearn *et al.* 2002; Montési 2004a; Perfettini & Avouac 2007). In subduction zones, several models have successfully described both transient post-seismic and steady interseismic deformation with only localized fault creep (e.g. Miyazaki & Heki 2001; Wang *et al.* 2003; Miyazaki *et al.* 2004; Norabuena *et al.* 2004; Bürgmann *et al.* 2005; Hsu *et al.* 2006; Suwa *et al.* 2006). Several post-seismic and interseismic models have been proposed which include only off-fault rheologies (e.g. Matsu'ura & Sato 1989; Suito & Hirahara 1999; Wang *et al.* 2001; Ogawa & Heki 2007), and several authors have concluded that off-fault rheologies may be important for steady interseismic deformation in subduction zones (e.g. Savage 1995; Wang 1995; Azúa *et al.* 2002). However, Thatcher & Rundle (1984) showed that surface deformation is similar in models with only off-fault viscoelasticity or only time-dependent fault creep, and many authors approximate off-fault rheologies at depth with fault zone creep (e.g. Wang *et al.* 2003; Perfettini *et al.* 2005; Wang 2007). The relative role of off-fault and fault zone deformation during the seismic cycle is an open question, and the success of a certain class of mechanical models to explain geodetic observations does not necessarily imply that the rheologies in those models are correct. Nevertheless, in this paper we assume that fault creep is the dominant mechanical response of the lithosphere, and that off-fault deformation at depth can be approximated by creep on a deep fault.

Several authors have proposed post-seismic models where creep is a function of the fault traction, including coseismic shear stress changes, and the rheological properties of the fault (e.g. Hearn *et al.* 2002; Johnson *et al.* 2006; Perfettini & Avouac 2007; Barbot *et al.* 2009). Researchers have also tested inferred post-seismic creep in kinematic models for consistency with fault rheologies (e.g. Miyazaki *et al.* 2004; Hsu *et al.* 2006). Post-seismic models containing only localized fault creep were motivated by the spring-and-slider post-seismic model of Marone *et al.* (1991), and some researchers continue to use spring-and-slider models to either describe post-seismic deformation or supplement 3-D models (e.g. Miyazaki *et al.* 2004; Montési 2004a; Perfettini *et al.* 2005; Hsu *et al.* 2006; Johnson *et al.* 2006, Fukuda *et al.* 2007). Spring-and-slider models are analytically and computationally simple, and thus are powerful tools for exploring a wide range of fault rheologies; however, spring-and-slider models lack the geometric complexity required to model surface deformation with a consistent model (e.g. Hetland & Hager 2006a; Johnson *et al.* 2006).

Most proposed 3-D post-seismic slip models do not attempt to describe the near steady interseismic deformation observed before earthquakes. Without prior knowledge of the initial conditions, authors often use simple, *ad hoc* physically based arguments to determine initial stresses. Alternatively, one could include the initial stresses as free parameters when describing the post-seismic observations. However, there are potentially strong trade-offs between pre-stresses and inferred rheological parameters, and ideally, the initial stresses in a post-seismic model should be a consequence of the long-term deformation of the system. In our model, the stresses at any time result from all past fault slip, and thus our model can be used to constrain fault rheologies from geodetic observations, using internally consistent initial conditions.

In this paper, we present and discuss our model formulation and assumptions, emphasizing the importance of various choices that must be made in our model, as well as the role of model spin-up, the size of the computational domain, and the pattern of interseismic creep for various fault rheologies. In a companion paper (Hetland & Simons, *Interseismic and Post-seismic Fault Creep II: Transient Creep and Stress Shadows on Megathrusts*; hereafter referred to as Paper 2), we use this model to illustrate interseismic strain accumulation in subduction zones under a variety of synthetic scenarios, and to investigate the mechanics of megathrusts during the interseismic period.

2 MODEL FORMULATION

Our interseismic creep model is based on a finite fault embedded in an elastic medium (Fig. 1). We do not differentiate between a fault plane or a finite thickness fault zone, and thus for fault zone thickness h and characteristic fault dimensions D, we assume that $h \ll D$. We consider both strike-slip and dip-slip fault creep. We assume a homogeneous Poisson half-space in all calculations in this paper, but our model formulation is valid for any Poisson ratio or linear elastic medium. In the following subsections, we separately

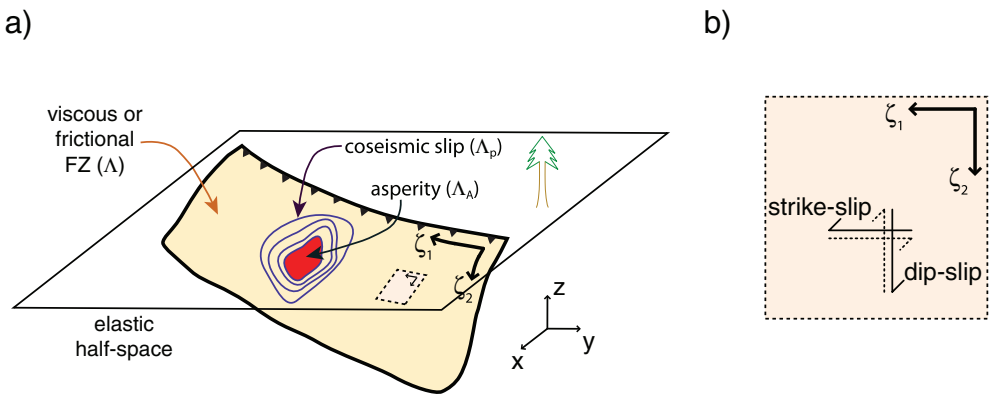

Figure 1. (a) Cartoon of fault model presented in this paper, including contours of coseismic slip and the location of an asperity; barbed line is the fault trace. (b) Blow up of fault patch shown in (a), with a locally orthogonal coordinate system.

Table 1. Model parameters: i or $j = s$, d or n denotes the components in the local strike-slip, dip-slip or fault normal directions.

D	Characteristic model dimension
h	Fault zone thickness
L_b	Critical fault dimension
L_τ	Dimension of coseismic traction perturbations on the fault
$s_i(\zeta, t)$	Aseismic fault creep
$s_i^\star(\zeta, t)$	Total coseismic slip and aseismic creep
s_o	Characteristic coseismic slip
$S_i(\zeta)$	Imposed coseismic fault slip
t	Time
T	Characteristic timescale
$v_i(\zeta, t)$	Creep rate, $\frac{ds_i}{dt}$
V_i	Fault loading rate
v_T	$= s_o/T$, characteristic slip rate
u_k	Surface displacements
w_k	Surface velocities
Λ	Finite fault plane (or fault zone)
Λ_∞	Semi-infinite extension of Λ
μ	Shear modulus
$\sigma_E(\zeta)$	Effective normal stress across the fault
$\tau_i(\zeta, t)$	Traction resolved on the fault
ζ	General fault coordinates

address fault traction, fault rheology, the numerical solution and the calculation of surface displacements.

2.1 Fault traction

For time-dependent fault slip or creep, $s_j^\star$ ($j = s$ or d representing strike- and dip-slip, respectively, and superscript $\star$ signifies that s includes both coseismic slip and aseismic creep; see Table 1 for list of model symbols), the ith component of the traction on the fault plane ($i = s$ or d representing shear traction on the fault in the strike or dip directions, or $i = n$ representing fault normal traction with $\tau_n > 0$ compressive) is

$$\tau_i(\zeta, t) = \int_\Lambda s_j^\star(\xi, t) K_{ji}(\zeta; \xi) \mathrm{d}\xi, \tag{1}$$

where K is the stress kernel, and Λ is an arbitrarily shaped finite fault, with general coordinates ζ, embedded in an elastic medium (Fig. 1a). The strike-slip direction is defined as the slip locally tangent to the fault plane and parallel to the surface, while the dip-slip component is orthogonal to the strike-slip direction (Fig. 1b).

Eq. (1) ignores fault loading, which can be introduced in two mathematically equivalent ways. For the first, we define the semi-infinite extension of Λ, Λ_∞, such that $\Lambda \cup \Lambda_\infty$ entirely cuts the elastic medium. Imposing that slip on Λ_∞ is uniform at the constant slip rate V_j, the fault traction on Λ is given by

$$\tau_i(\zeta, t) = \int_\Lambda s_j^\star(\xi, t) K_{ji}(\zeta; \xi) \mathrm{d}\xi + \int_{\Lambda_\infty} t\, V_j K_{ji}(\zeta; \xi) \mathrm{d}\xi. \tag{2}$$

For planar faults and constant slip S, $\int_\Lambda SK \mathrm{d}\xi + \int_{\Lambda_\infty} SK \mathrm{d}\xi = 0$, which states that constant fault offset does not result in an accumulation of stress. Assuming the cumulative fault offset over many earthquakes does not result in an accumulation of stress, we can rearrange eq. (2) as

$$\tau_i(\zeta, t) = \int_\Lambda [s_j^\star(\xi, t) - t\, V_j] K_{ji}(\zeta; \xi) \mathrm{d}\xi, \tag{3}$$

and thus, τ is given by integration only over the finite fault, with $s - tV$ being the so-called back-slip, a common fault loading condition used in dynamic earthquake models (e.g. Rice 1993; Lapusta & Rice 2003; Liu & Rice 2005; Hillers & Wesnousky 2008; Perfettini & Ampuero 2008). An alternative is to load the fault by far-field boundary conditions, but in this model we only consider faults loaded via back-slip—we remark further on this restriction later.

Eq. (3) is the basic equation of motion introduced by Rice (1993), although he augmented it by including a damping term that approximates dynamic effects due to radiation of seismic energy (Rice 1993; Ben-Zion & Rice 1995). The damping term limits fault slip rates from becoming unbounded during earthquake calculations (e.g. Rice 1993; Lapusta *et al.* 2000), and because we are only concerned with fault creep at subseismic rates, we do not include radiation damping.

We explore the class of models in which given regions of the fault only slip during earthquakes. We refer to the regions where the accumulated slip deficit due to fault loading is entirely accommodated by earthquakes as 'asperities'. Our definition of asperities is based on the common usage in seismology (e.g. Aki 1984; Kanamori 1986; Bilek & Lay 2002), although we restrict our definition to refer to regions with no, or negligible, interseismic creep. We use 'transition regions' to refer to regions of the fault that experience both significant coseismic slip and interseismic creep. The locations of asperities are not explicitly defined during model setup, rather they are implicit through our specification of the coseismic slip history and fault loading. In general, we solve for interseismic creep over the entire fault plane, although to simplify calculations, we often do not solve for creep within the entire asperities which do not creep between imposed earthquakes. We denote coseismic slip in the j direction and in the pth earthquake as $S_{jp}(\zeta, t)$, which we assume is instantaneous. Our methodology is applicable to the imposition of time-dependent slip in the quasi-static approximation (i.e. slow slip episodes), although we do not consider such imposed slip here. Including unknown interseismic creep, s_j, imposed coseismic slip, and fault-loading via back-slip, traction on the fault becomes,

$$\tau_i(\zeta, t) = \int_\Lambda s_j(\xi, t) K_{ji}(\zeta; \xi) \mathrm{d}\xi + \sum_p \int_\Lambda S_{jp}(\xi, t) K_{ji}(\zeta; \xi) \mathrm{d}\xi - \int_\Lambda t\, V_j K_{ji}(\zeta; \xi) \mathrm{d}\xi. \tag{4}$$

2.2 Fault rheologies

The traction on the fault, $\tau_i(\zeta, t)$, is related to the creep rate of the fault, $v_i(\zeta, t)$, through the fault rheology. To determine the fault creep and creep rate, we simultaneously solve eq. (4) and the fault constitutive equation, assuming co-linearity of fault traction and creep rate. We consider four fault rheologies: linear viscous, non-linear viscous, rate-dependent friction and rate- and state-dependent friction—we refer to the latter two rheologies simply as 'RD friction' and 'RS friction'. We non-dimensionalize by the shear modulus, μ, a model dimension, D, a slip distance, s_o, a time, T, and a slip rate, v_T, and we denote the non-dimensionalized variables with a prime (Table 2). Typically, D is a characteristic dimension of an asperity, s_o is a characteristic coseismic slip, T is a characteristic earthquake recurrence time, and $v_T = s_o/T$ is the fault loading rate (i.e. the far field velocity).

2.2.1 Linear viscous

The simplest fault rheology is the linear relation

$$v(\zeta, t) = \tau(\zeta, t)/\alpha_1(\zeta), \tag{5}$$

© 2010 The Authors, *GJI*, **181,** 81–98
Journal compilation © 2010 RAS

Table 2. Non-dimensional model parameters.

s'	=	s/s_o	t'	=	t/T
L'	=	L/s_o	L'_b	=	L_b/D
L'_τ	=	L_τ/D	v'	=	$v/v_T = vT/s_o$
w'	=	w/v_T	α'	=	$\alpha D/\mu s_o$
σ'	=	$\sigma D/\mu s_o$	θ'	=	θ/T
τ'	=	$\tau_i D/\mu s_o$	ζ'	=	ζ/D

Notes: D is a characteristic dimension of an asperity or an earthquake, s_o is a characteristic coseismic slip, T is a characteristic earthquake recurrence time and $v_T = s_o/T$ is the fault loading rate.

Table 3. Notation used to describe fault rheological parameters.

	Viscous rheologies
n	Exponent of non-linear viscous rheology, $n = 1$ is linear viscous
α_1	Strength term in linear viscous rheology ($\alpha_1 = \eta/h$)
α_n	Strength term in non-linear viscous rheology
η	Fault zone viscosity
	Frictional rheologies
a, b	RS friction material properties
f	Fault friction
f_o	Reference fault friction
L	Characteristic slip distance in RS friction
v_o	Reference slip velocity in frictional fault rheologies
α	$= a\sigma_E$ in RS friction
α_h	$=(a-b)\sigma_E$ in RD friction
γ	$= b/a$
Ω	$=\lvert v\rvert\theta/L$
ρ	$= f_o/a$ in RS friction
ρ_h	$= f_o/(a-b)$ in RD friction
θ	RS friction state variable

Note: See Table 2 for non-dimensional variables.

where α_1 is a parameter controlling the strength of the fault (see Table 3 for notation of fault rheological parameters). For a fault zone of thickness h and viscosity η, $\alpha_1 = \eta/h$, and a decrease in α_1 is equivalent to a decrease in the fault zone viscosity, and results in larger creep rates for a given fault traction (e.g. Hearn *et al.* 2002; Montési 2004a). (Note that we assume that $h \ll D$, and neither h nor η are explicitly included in these calculations.) In general, α_1 might depend on the effective fault normal traction as well, but we do not consider it here. In non-dimensional form

$$v'(\zeta', t') = \tau'(\zeta', t')/\alpha'_1(\zeta'), \tag{6}$$

where

$$\alpha'_1 = \alpha_1 v_T \frac{D}{\mu s_o} = \frac{D}{h}\frac{\eta}{T\mu}. \tag{7}$$

The parameter α'_1 is similar to the inverse of the Savage parameter, which is defined for models of a faulted elastic layer over a Maxwell viscoelastic half-space, and is the ratio of the earthquake recurrence time to the steady relaxation time of the lithosphere (Savage & Prescott 1978; Hetland & Hager 2006b).

2.2.2 Non-linear viscous

The next level of complexity in a fault rheology is the non-linear viscous, or power-law, rheology. The non-linear viscous rheology was proposed by Montési & Hirth (2003) as appropriate for ductile shear zones, where the effective viscosity of the fault zone decreases at high traction. Montési & Hirth (2003) also considered grain size to vary in response to traction; however, in this paper we follow Montési (2004a) and consider a simplified form of the non-linear viscous rheology. Montési (2004a) argued that this rheology is appropriate to post-seismic timescales, and using a 1-D spring-and-slider model, he successfully fit geodetic time-series following several continental and subduction zone earthquakes. A non-linear viscous fault rheology can be expressed as

$$v(\zeta, t) = \tau^n(\zeta, t)/\alpha_n(\zeta), \tag{8}$$

where n is a constant, and α_n effectively controls the strength of the fault. When $n = 1$, the non-linear viscous rheology reduces to the linear viscous rheology. The non-dimensional form of eq. (8) is as in eq. (6), with

$$\alpha'_n(\zeta') = \alpha_n v_T \left(\frac{D}{\mu s_o}\right)^n. \tag{9}$$

2.2.3 Rate-dependent friction

RD friction is occasionally referred to as 'hot friction' by some researchers (e.g. Linker & Rice 1997; Hearn *et al.* 2009), as it may be appropriate for high temperature faults. RD friction is a restricted form of RS friction, hence it is often considered after RS friction is introduced. However, in this paper we discuss RD friction before RS friction (we refer readers to Rice & Gu 1983; Marone *et al.* 1991) for the derivation of RD friction from RS friction). Marone *et al.* (1991) first proposed an RD friction fault rheology in a spring-and-slider model to explain geodetic observations of post-seismic deformation following the 1966 Parkfield earthquake, although several researchers have subsequently appealed to RD friction in 3-D models of post-seismic deformation (e.g. Hearn *et al.* 2002, 2009; Perfettini & Avouac 2004; Barbot *et al.* 2009). Montési (2004a) demonstrated that a spring-and-slider model with a non-linear viscous rheology is the same as the deformation in an RD frictional model when $n \to \infty$.

In RD friction, the relationship between fault creep rate and traction is

$$v(\zeta, t) = \mathrm{sgn}\{\tau(\zeta, t)\}\, v_o \exp\left\{\frac{-f_o}{a-b}\right\} \exp\left\{\frac{|\tau(\zeta, t)|}{(a-b)\sigma_E(\zeta)}\right\}, \tag{10}$$

where v_o and f_o are a reference velocity and friction, respectively, a and b are dimensionless constants, and σ_E is the effective normal stress across the fault (e.g. Marone *et al.* 1991). a, b and f_o can vary over the fault, but for simplicity we do not write them as spatial functions. In general, σ_E is also a function of time, given by $\sigma_E(\zeta, t) = \sigma_o(\zeta) + \tau_n(\zeta, t)$, where σ_o is a nominal normal stress (including both lithostatic stresses and fault pore pressures) and τ_n is the change in normal traction due to fault slip, as defined in eq. (4). Indeed, time-dependent slip on a fault leads to variations in normal traction on portions of the fault, and these variations may be significant, particularly in subduction zones (e.g. Wang & He 2008). When $a - b < 0$, an increase in v corresponds to a decrease in τ, and the fault is velocity weakening, and when $a - b > 0$, increasing v corresponds to increasing τ, and the fault is velocity strengthening (e.g. Scholz 1998).

Eq. (10) leads to the unphysical behaviour that $v(\tau = 0) \neq 0$ and $v(\tau = 0^+) \neq v(\tau = 0^-)$, which we avoid by replacing $\exp\{\tau/(a-b)\sigma_E\}$ with $2\sinh\{\tau/(a-b)\sigma_E\}$ in eq. (10) (e.g. Rice & Ben-Zion 1996; Lapusta *et al.* 2000). The functional change is motivated by thermally activated creep at low traction (e.g. Rice *et al.* 2001), and is only important for $|\tau| < (a-b)\sigma_E$. Defining $\alpha_h \equiv (a-b)\sigma_E$ and $\rho_h \equiv f_o/(a-b)$, and replacing $\exp\{\ldots\}$ with $2\sinh\{\ldots\}$, eq. (10) becomes

$$v(\zeta, t) = 2v_o e^{-\rho_h(\zeta)} \sinh\left\{\frac{\tau(\zeta, t)}{\alpha_h(\zeta)}\right\}. \tag{11}$$

Taking the reference velocity as the model characteristic fault slip rate ($v_o = v_T$), and where $\alpha'_h = (a - b)\sigma'_E$, the non-dimensional form of RD friction is

$$v'(\zeta', t') = 2e^{-\rho_h(\zeta')} \sinh\left\{\frac{\tau'(\zeta', t')}{\alpha'_h(\zeta')}\right\}. \quad (12)$$

For a given fault traction, the slip rate decreases as α'_h increases, and thus α'_h can be viewed similar to α'_n in the viscous rheologies above. The average traction supported on a mature fault is given by $\alpha'_h\rho_h$, although α'_h has a greater effect on the variation of creep throughout the interseismic period. Laboratory studies suggest $(a - b) \approx 10^{-2}$ (e.g. Blanpied *et al.* 1991; Marone 1998a), and taking $f_o \approx 0.1$–1, $\rho_h \approx 10$–100. The effective normal traction on a fault is usually assumed to be of order 10^1–10^2 MPa (e.g. Rice 1993; Lapusta & Rice 2003), so $\alpha_h \approx 10^5$–10^6 Pa. Assuming $\mu \approx 10^{10}$ Pa, $s_o \approx 10$ m and $D \approx 10^4$ m, $\alpha'_h \approx 10^{-2}$–$10^{-1}$.

2.2.4 Rate-state friction

RS friction was developed empirically (e.g. Dieterich 1979; Ruina 1983), and has been described in detail by numerous researchers (see references in Marone 1998a; Rice *et al.* 2001). The majority of studies have focused on the velocity weakening regime and the earthquake process itself, although there are some notable exceptions, including Perfettini & Ampuero (2008) and Helmstetter & Shaw (2009). In RS friction, the fault friction, f, is given by

$$f = f_o + a \ln\left\{\frac{v}{v_o}\right\} + b \ln\left\{\frac{v_o\theta}{L}\right\}, \quad (13)$$

where θ is a frictional state parameter, L is a state evolution distance, f_o and v_o are reference friction and velocity, respectively, and a and b are material parameters. For our purposes it is useful to consider the inverse of eq. (13). Noting that $\tau = f\sigma_E$ and accounting for creep at low traction, we find

$$v(\zeta, t) = 2v_o e^{-\rho(\zeta)} \sinh\left\{\frac{\tau(\zeta, t)}{\alpha(\zeta)}\right\} \left[\frac{v_o\theta(\zeta, t)}{L(\zeta)}\right]^{-\gamma(\zeta)}, \quad (14)$$

where we define $\rho \equiv f_o/a$, $\alpha \equiv a\sigma_E$ and $\gamma \equiv b/a$.

The evolution of the state variable can be described by the so-called 'slip law' or 'aging law' (e.g. Marone 1998a). The slip law may be a more appropriate representation of the state evolution during earthquake nucleation and slip (e.g. Ampuero & Rubin 2008), while the aging law may be more appropriate to describe the state evolution during interseismic periods (e.g. Marone 1998a). Throughout this study, we do not consider earthquake nucleation or slip during earthquakes, so we only consider the aging law, given by

$$\frac{\partial\theta(\zeta, t)}{\partial t} = 1 - \frac{|v(\zeta, t)|\theta(\zeta, t)}{L(\zeta)} \quad (15)$$

(see references in Marone 1998a).

For velocity strengthening (weakening), $\gamma < 1$ ($\gamma > 1$). Both α and ρ have similar roles as α_h and ρ_h in RD friction, where $\alpha_h = \alpha(1 - \gamma)$, $\rho_h = \rho/(1 - \gamma)$, and $\alpha_h\rho_h = \alpha\rho$. We discuss the role of L and γ later. Taking $v_o = v_T$, the non-dimensional forms of eqs (14) and (15) are

$$v'(\zeta', t') = 2e^{-\rho(\zeta')} \sinh\left\{\frac{\tau'(\zeta', t')}{\alpha'(\zeta')}\right\} \left[\frac{\theta'(\zeta', t')}{L'(\zeta')}\right]^{-\gamma(\zeta')} \quad (16)$$

and

$$\frac{\partial\theta'(\zeta', t')}{\partial t'} = 1 - \frac{|v'(\zeta', t')|\theta'(\zeta', t')}{L'(\zeta')}, \quad (17)$$

where $\theta' = \theta/T$, $L' = L/s_o$, $\alpha' = a\sigma'_E$, and all other terms are as defined above. Roughly $a \approx 0.015$ and $(a - b) \approx 0.000$–0.015 in velocity strengthening regions, so that b varies between 0.000 at depth and 0.015 at the surface (Blanpied *et al.* 1991), so $\rho \approx 10$–100 assuming $f_o \approx 0.1$–1. For $\sigma_E \approx 10^1$–10^2 MPa, $s_o \approx 10$ m, and $D \approx 10^4$ m, $\alpha \approx 10^5$–10^6 Pa and $\alpha' \approx 10^{-2}$–10^{-1}. L has been inferred to be about 10^{-6}–10^{-4} m in experimental studies (e.g. Marone 1998a), although Marone & Kilgore (1993) suggested that L may be of order 10^{-2} m in natural faults. Some researchers have argued that the experimental values are more appropriate for natural faults (e.g. Lapusta & Rice 2003), and Tinti *et al.* (2009) pointed out that determination of L from records of earthquakes is an ongoing problem. Assuming $s_o \approx 10$ m and L between 10^{-6} and 10^{-2} m, L' is about 10^{-7}–10^{-3}. In practice, calculations with L' this low are too computationally burdensome (see also discussions in Rice 1993; Lapusta & Rice 2003), and we take $L' > 10^{-2}$ for most of the models we consider. We explore the assumption of using such large values of L' below. When $\frac{\partial\theta'(\zeta', t')}{\partial t'} \ll 1$, $\Omega \equiv \theta' v'/L' \approx 1$ and for $|\tau'| > \alpha'$ eq. (16) is approximately eq. (12) with $\rho_h = \rho/(1 - \gamma)$ and $\alpha'_h = \alpha'(1 - \gamma)$. We also note that α' is in general a function of time since $\sigma'_E(\zeta', t') = \sigma'_o(\zeta') + \tau'_n(\zeta', t')$, where σ'_o is a nominal normal traction and $\tau'_n(\zeta', t')$ is the normal traction on the fault due to fault slip.

2.3 Numerical solution

We use the analytic expressions of Okada (1992) to determine K for a spatially discretized fault in a homogeneous Poisson elastic half-space. The solution of Okada (1992) is for rectangular dislocations, and in this paper we only consider planar faults that are discretized using rectangular patches. For non-planar faults in an elastic half-space, we could use the analytic expressions for triangular dislocations given by Meade (2007) in order to calculate K, although K could also be determined using point sources, propagator matrix methods, boundary element models, or finite element models. We evaluate K at the centre points of the discretized fault cells, and we solve a discretization of eq. (4), together with the fault constitutive equation, for creep during the interseismic period. We use a Runge–Kutta method with variable time stepping to evolve the system of equations through time (e.g. Dormand 1996; Noda *et al.* 2009). With this technique, time steps decrease (increase) as creep rates increase (decrease), and variable time steps lower the computational cost of the solution dramatically. All calculations in this paper are done using Matlab.

2.4 Surface displacements

Once we know the fault slip through time, we can determine the time-dependent surface displacements by

$$u_i(x, t) = \int_\Lambda s^\star_j(\xi, t)G_{ji}(x, \xi)\mathrm{d}\xi + \int_{\Lambda_\infty} tV_j G_{ji}(x, \xi)\mathrm{d}\xi, \quad (18)$$

where G_{ji} are Green's functions. We use a discretized form of eq. (18) corresponding to the discretization of eq. (4), and G_{ji} is determined in the same way as K_{ji}. The cumulative surface displacements over many mature seismic cycles predicted by eq. (18) is block-like deformation across the fault. In this paper, we only consider strike-slip faults, although our model is also applicable to reverse faults. For reverse faults, block-like deformation is uplift of the hanging-wall relative to the footwall (Fig. 2a). On the other hand, the cumulative deformation expected in a subduction system does

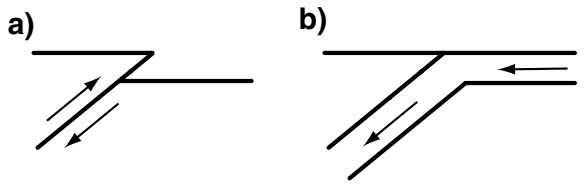

Figure 2. Cartoons of the cumulative block-deformation in a continental thrust fault (a) and subduction system (b).

not have any net vertical offset across the trench (Fig. 2b). Long-term subduction block-like motion can be achieved by including dislocations that are assumed to approximate the deformation at the base of the subducting elastic plate (Kanda & Simons 2010). Kanda & Simons (2010) show that if the plate bending stresses are either negligible or are released continuously throughout the seismic cycle, then the predicted surface deformation on the arc-side is identically equal to the surface deformation given by the equivalent back-slip (the surface displacements on the plate-side differ by a constant offset). Hence, for the surface deformation on the arc-side of a subduction system, we subtract slip due to fault loading from (18) to give

$$u_i(x,t) = \int_{\Lambda} [s_j^{\star}(\xi,t) - tV_j] G_{ji}(x,\xi) \mathrm{d}\xi. \tag{19}$$

Note that, in contrast to the traction on the fault, $\int_{\Lambda} SG\mathrm{d}\xi + \int_{\Lambda_\infty} SG\mathrm{d}\xi = \mathcal{U}$ for constant slip S, and in general $\mathcal{U} \neq 0$. In other words, complete slip of a plane bisecting an elastic half-space does not result in zero surface deformation. In the model of Kanda & Simons (2010), $\mathcal{U} = 0$ on the arc-side for all components of deformation, while on the plate-side, $\mathcal{U} = 0$ for the vertical components and $\mathcal{U} = V$ for the trench normal horizontal component.

3 SPIN-UP, COSEISMIC SLIP AND MODEL DOMAIN

We explore several features of our model formulation, including model spin-up, imposed coseismic slip and finite fault size. For illustrative purposes, we only consider 2-D vertical strike-slip faults, with infinite length aligned along the x-axis, in all calculations in this paper. The application of this model to 3-D reverse faults is presented in Paper 2. For simplicity, we drop the subscript s on all model results, and it is understood that they are in the fault strike-slip component. We periodically impose an earthquake, with period T, and we assume that coseismic slip is uniform within the asperities with magnitude of s_o, and tapers to zero outside of the asperities. We load the fault by steady creep at rate $v_T = s_o/T$ below $z' = -14$. This depth is sufficiently deep such that the model results are not artificially affected by the imposed steady creep (see Section 3.3).

3.1 Model spin-up

After a series of imposed earthquakes, the model matures and interseismic creep is no longer dependent on initial conditions; we refer to this process as model spin-up. In the case of periodic earthquakes in time, the model spins-up such that the deformation throughout the interseismic period is cycle invariant (i.e. the same in all seismic cycles). Because we neglect instabilities associated with earthquake rupture nucleation and we only consider velocity strengthening rheologies, all of the models that we explore have a cycle invariant state.

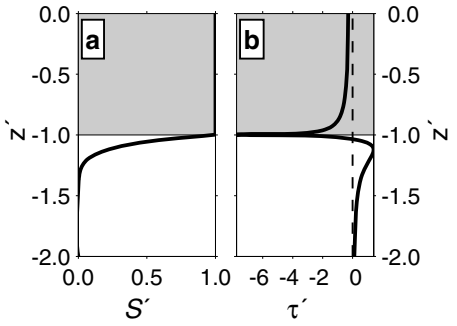

Figure 3. (a) Coseismic slip, S', on a 2-D strike-slip fault. (b) Coseismic fault traction, τ', due to slip in (a). Shaded region in both panels signifies the asperity.

The concept of spin-up also holds for non-periodic earthquake sequences, as long as the cumulative coseismic slip over some number of seismic cycles equals slip due to fault loading. Spin-up can be thought of as the time required for the regions of the model away from the asperities and fault boundaries to equilibrate with the model forcings (applied coseismic slip and fault loading). Models with stronger faults, or with greater distances between the boundaries and the asperities, take longer to spin-up. While all models shown in this paper assume periodic earthquakes, our model formulation is applicable to non-periodic earthquake sequences. Spin-up in these models is qualitatively similar to spin-up in layered viscoelastic models, and we refer readers to Hetland & Hager (2006b) for a discussion of spin-up in models with viscoelastic rheologies and either periodic or non-periodic earthquake sequences. We spin-up these models by repeated application of coseismic slip; however, models in which coseismic slip is kinematically imposed once a stress threshold has been reached, also spin-up in a similar fashion (DiCaprio *et al.* 2008).

We demonstrate spin-up from an initially unstressed fault, using a 2-D strike-slip model with the coseismic slip distribution in Fig. 3(a). By the nomenclature used in this paper, we refer to the depth range $-1 < z' < 0$ as the model asperity, because at these depths imposed coseismic slip is sufficient to match the fault loading. This coseismic slip distribution is chosen somewhat arbitrarily so that the traction due to the coseismic slip is bounded (see Section 3.2). Over a small region of the fault closest to the asperity, the traction following coseismic slip may be negative (Fig. 3b), and the fault may post-seismically creep opposite to the sense of coseismic slip. However, once spun-up, any regions of negative traction and creep become negligible.

In Fig. 4, we show the evolution of fault traction during the spin-up of models with linear viscous, non-linear viscous, RD friction, and RS friction fault rheologies. Our purpose here is not to compare different fault rheologies, rather, we choose the rheological parameters arbitrarily for clarity of the figures. During spin-up, the fault traction adjusts from the initial conditions to the cycle invariant fault traction. Once the model matures, the cycle invariant traction on the fault varies throughout the interseismic period, and the traction at the end of an entire seismic cycle is identical to the traction prior to the previous earthquake in that cycle. In a model with an RS frictional fault, the state variable also evolves as the model spins-up, and once fully spun-up, θ falls into the quasi-steady state of cycle invariance (Fig. 4c). The time average cycle invariant fault traction, τ_{steady}, is the traction required for the fault to creep steadily at v_T. For viscous faults, $\tau_{\text{steady}} = (\alpha_n')^{1/n}$, for RD friction faults, $\tau_{\text{steady}} = \rho_h \alpha_h'$, and

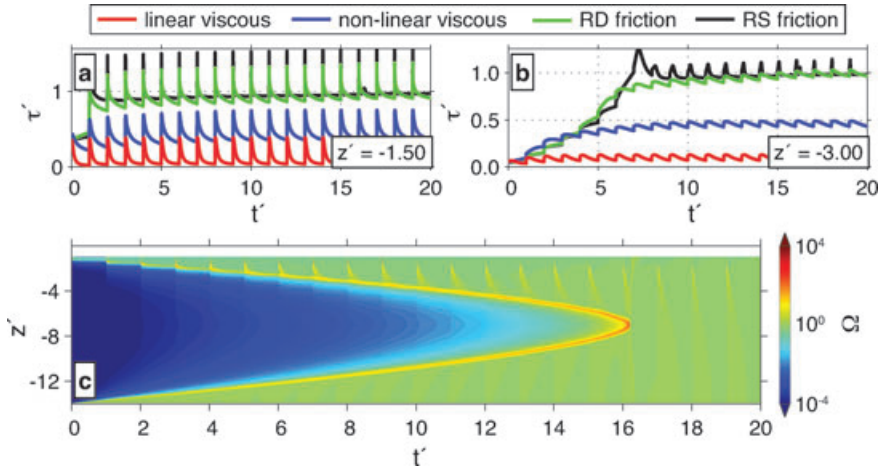

Figure 4. (a) and (b) Shear traction on the fault during spin up at $z' = -1.5$ (a) and $z' = -3.0$ (b) in models with a linear viscous ($\alpha'_1 = 0.1$), non-linear viscous ($\alpha'_3 = 0.1$, $n = 3$), RD frictional ($\rho_h = 10$, $\alpha'_h = 0.1$), or RS frictional ($\rho = 10$, $\alpha' = 0.1$, $L' = 0.05$, $\gamma = 0.9$) fault rheologies. (c) Ω during spin-up of the RS frictional model. Model geometry and coseismic slip are shown in Fig. 3(a).

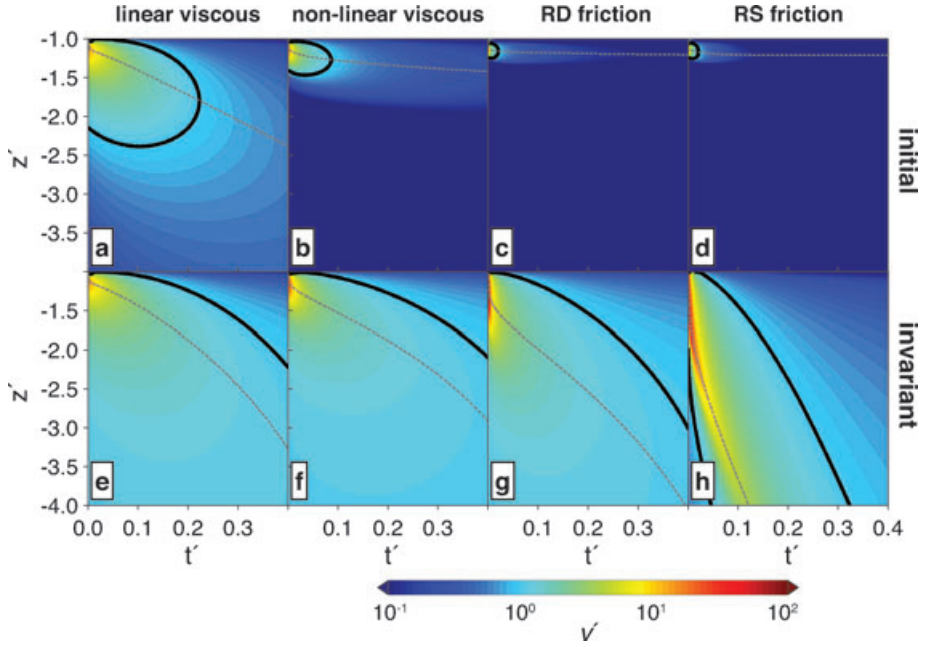

Figure 5. Fault creep rate in models depicted in Fig. 4, during the initial (a–d) and mature (e–f) seismic cycles. Black solid lines are the $v' = 1$ isovelocity contours (i.e. velocity is equal to the long term plate rate), and dotted lines indicate the depth of the maximum creep rate at each time step.

for RS friction fault, $\tau_{\text{steady}} = \rho\alpha'$. Initially pre-stressing the fault at τ_{steady} reduces the spin-up time to a few seismic cycles.

During spin-up, the behaviour of fault creep also changes, both spatially and temporally. Initially after the first earthquake, post-seismic creep is localized near the asperity, with a greater degree of localization in models with non-linear fault rheologies (both viscous and frictional; Fig. 5). In a mature seismic cycle there is larger post-seismic creep away from the asperities than in cases when the model is not spun-up (Fig. 5). In models with non-linear fault rheologies, the post-seismic creep in a mature cycle varies less rapidly than in the initial cycle (Fig. 5), because in a mature cycle the traction before the earthquake is larger than in the initial cycle (Fig. 4). Once spun-up, post-seismic creep forms a spatio-temporal creep pulse (Figs 5e–h). The speed with which the pulse propagates away from the coseismic slip, and the spatial breadth of the pulse, depend mainly on the type of fault rheology, although the rheological parameters also affect the spatio-temporal pattern of post-seismic creep (we explore the dependence of the post-seismic creep on rheological parameters in Section 4). Later in the interseismic period, as the post-seismic creep pulse propagates away from the asperity, the fault creeps at a rate below the loading rate near the asperity. This slowing of the creep rates late in a seismic cycle can result in the fault appearing locked over a region larger than the eventual coseismically active region. We remark further on the time-dependent expansion of apparent fault locking and its implication on subduction zone studies in Paper 2.

3.2 Imposed coseismic slip

It is unlikely that during an earthquake there is only coseismic slip within asperities, although the extent that coseismic slip extends into non-asperity regions depends on the frictional properties in

© 2010 The Authors, *GJI*, **181,** 81–98
Journal compilation © 2010 RAS

and at the edges of the asperities (e.g. Boatwright & Cocco 1996; Lapusta & Rice 2003; Tinti *et al.* 2005; Hillers & Wesnousky 2008). In our model, we apply coseismic slip in asperities, and we can taper coseismic slip into non-asperity regions. Large spatial gradients in coseismic slip lead to large coseismic traction change, and in the extreme case where we apply uniform coseismic slip only within the asperity, the traction is singular at the asperity boundaries (e.g. Okada 1992). Large traction resulting from unphysically large spatial gradients in imposed coseismic slip, result in unphysically high post-seismic creep rates. We do not interpret these high creep rates to have any geophysical meaning, and their result is to rapidly smooth out artificially large gradients in coseismic slip. Indeed, the exact pattern of coseismic slip depends on the frictional properties of the fault, and the heterogeneous properties in the velocity strengthening regions adjacent to velocity weakening regions has a strong influence on the amount coseismic slip extends into the velocity strengthening regions (e.g. Boatwright & Cocco 1996; Tinti *et al.* 2005; Hillers & Wesnousky 2008).

For spatially discontinuous coseismic slip imposed in these models, the immediate post-seismic creep rates can be more than $10^{10} v_T$, which is roughly 10 m s^{-1} for $v_T = 3$ m/100 yr. Average seismic slip rates are usually observed to be about 1 m s^{-1} (e.g. Heaton 1990), which is about $10^9 v_T$, assuming $v_T = 3$ m/100 yr. The extremely high creep rates resulting from discontinuous coseismic slip are localized near large coseismic slip discontinuities, and commonly by about $t' = 10^{-6}$ the creep rates decrease to reasonable post-seismic creep rates (for a 100 yr earthquake repeat time, $t' = 10^{-6}$ is roughly one hour). Note that the exact time at which post-seismic creep rates fall to reasonable values, depends on the fault rheology and the imposed coseismic slip.

In a model with a discontinuous coseismic slip profile, an increase in mesh density is required to resolve the large gradients in traction, and the time steps need to be sufficiently small in order to resolve the rapid creep rates. Both the increased mesh density and the number of time steps lead to exceedingly large computation times. The computational burden can be significantly lessened by arbitrarily bounding the creep rates, and except during the immediate post-seismic period, the fault deformation is the same in computations with creep rates unbounded or bounded. In general, we recommend assuming coseismic slip distributions which lead to bounded post-seismic creep rates.

3.2.1 *Trade-off between coseismic slip and fault rheology*

As discussed above, large gradients in imposed coseismic slip result in large changes in fault traction, leading to large post-seismic creep rates which tend to smooth out the coseismic slip distribution. One may speculate that we should always impose discontinuous coseismic slip, and let the model adjust the coseismic slip to a physically reasonable coseismic slip distribution during some short period of time following the earthquake—we refer to this as the 'adjusted coseismic slip.' However, in models with RS frictional faults, the deformation after the adjustment period in the original model is not the same as in a model in which the adjusted coseismic slip was imposed. One may also speculate that there is a significant trade-off between imposed coseismic slip and fault rheology. In Section 4, we show that increasing α' results in less variation of interseismic creep (i.e. with less transient post-seismic creep), and increasing α' can represent either an increase in the frictional parameter a, or an increase in σ'_E. In this subsection, we demonstrate the impact of using adjusted coseismic slip and the potential trade-off between coseismic slip and fault rheology. We use a 2-D strike-slip fault model, with an asperity extending from the surface to $z' = -1$, and an RS friction fault rheology ($\gamma = 0.9$, $\rho = 10$, $L' = 0.05$ and α' as indicated below). We consider four coseismic slip distributions, and we present only the cycle invariant deformation (i.e. in spun-up models, assuming periodic earthquakes)

Coseismic slip in the first model we consider does not appreciably extend past the edge of the asperity (model 1; Fig. 6a), and thus the coseismic stresses are relatively large near the asperity (Fig. 6b). We set $\alpha' = 0.10$ in model 1, and the surface velocities predicted by model 1 are large in the immediate post-seismic period, and decrease rapidly (Figs 6c–e). In the second model, we apply coseismic slip that is the combination of the coseismic slip in model 1 plus the cumulative post-seismic creep during the first $t' = 10^{-6}$ following an earthquake in model 1 (model 2; Fig. 6a). Because the coseismic slip

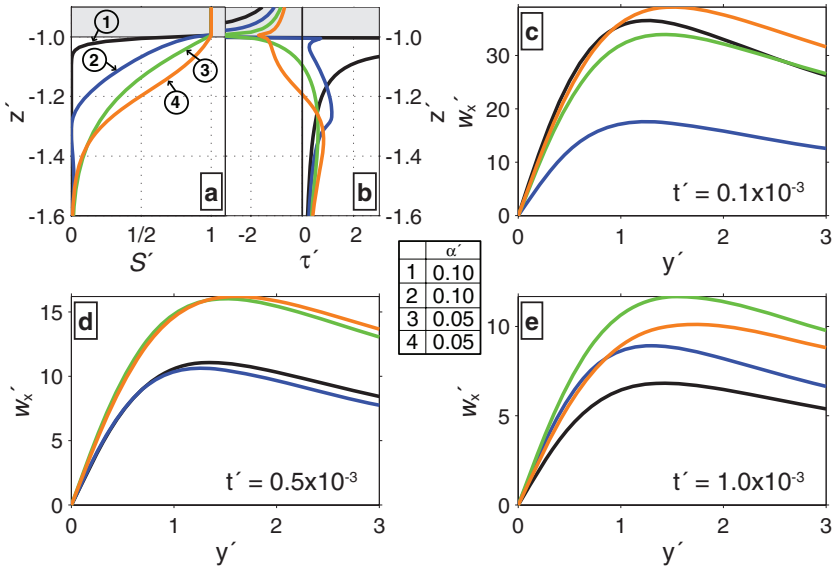

Figure 6. Coseismic slip (a), coseismic traction change (b), and cycle invariant fault parallel surface velocities at three different times (c–e) in 2-D strike-slip models with RS frictional faults ($\gamma = 0.9$, $\rho = 10$, $L' = 0.05$ and $\alpha' = 0.10$ in models 1 and 2, or 0.05 in models 3 and 4); y' is distance from the fault along the surface.

in model 2 is the total creep after some adjustment period of model 1, the coseismic slip in model 2 extends slightly father from the asperity compared to in model 1. Similarly, the coseismic traction is lower in model 2 compared to model 1 (Fig. 6b). The instantaneous fault traction at $t' = 10^{-6}$ in model 1 is identical to the traction at $t' = 0^{+}$ in model 2 (i.e. immediately after an earthquake); however, with $\alpha' = 0.10$ in both models, the surface velocities are not the same in models 1 and 2 (Figs 6c–e). In model 2, the velocities are lower immediately after the earthquake, and decay slower than in model 1. This difference stems from the fact that θ' immediately following the coseismic slip in model 2 is not the same as θ' after the adjustment period in model 1.

In a third coseismic slip distribution, we taper the coseismic slip to zero over a broader region of the fault compared to the previous models (model 3; Fig. 6a). As a result of the lower gradient in coseismic slip, the coseismic traction is lower than those in models 1 or 2 (Fig. 6b). To offset the lower coseismic traction, we set $\alpha' = 0.05$ in model 3, resulting in a similarity of the early post-seismic surface velocities to those in model 1 (Fig. 6c). However, the surface velocities decrease more slowly in time than in model 1, so that later in time the surface velocities in model 3 are larger than in model 1 (Figs 6d and e).

In the fourth coseismic slip model we consider, the coseismic slip tapers to zero over approximately the same region of the fault as in model 3, but with a slightly less severe taper near the asperity (model 4; Fig. 6a). Away from the asperity, the magnitudes of coseismic traction are similar in models 3 and 4, although the traction is fairly dissimilar closer to the asperity (Fig. 6b). We set $\alpha' = 0.05$ in models 3 and 4, and even with the slight difference in the taper of the coseismic slip, the surface velocities are fairly similar (Fig. 6c–e). By about $t' = 0.01$ the surface velocities in all four models are similar. By about $t' = 0.1$ the surface velocities are close to those in the elastic strain accumulation model of Savage & Burford (1973), and then decrease slowly during the rest of the interseismic period.

To summarize, when only considering surface deformation over a short time period, there may be trade-offs between coseismic slip and fault rheology, which may pose a problem because in general, the coseismic slip distribution in any particular event may be fairly uncertain (e.g. Simons *et al.* 2002; Chlieh *et al.* 2007; King & Wesnousky 2007). However, these trade-offs can be substantially minimized when considering deformation over a longer time period, as both the magnitudes and the variations through time of surface velocities are sensitive to fault rheology. The ideal case would be to consider both transient post-seismic deformation following an earthquake and steady interseismic deformation prior to that earthquake. Nevertheless, when comparing model results to actual observations, one should account for uncertainties in the assumed coseismic slip when inferring fault rheology from surface deformation.

3.3 Influence of fault domain

In our model formulation, we only calculate slip on a finite fault, Λ, and we assume that the semi-infinite extension of the fault slides steadily at the fault loading rate, v_T. As described in Section 3.1, the distance from the asperities to the model boundaries affects the spin-up time of the model. When Λ is only slightly larger than the asperities, the model spins-up in fewer seismic cycles than for larger fault domains. Hence, limiting Λ decreases computation cost not only because fewer fault elements are needed to represent the fault, but also because the model spins-up in less time steps. However, in these calculations limiting Λ may strongly affect the model results. We illustrate this point with a 2-D model of a strike-slip fault, in which we impose periodic earthquakes, with period T and uniform slip s_o from $z' = -0.5$ to -1.5, and slightly tapered above and below the asperity (Fig. 7a). Λ always extends to the free surface, and we vary the depth of the lower boundary of Λ.

We assume the non-asperity regions of the fault are described by RS friction, with $L' = 0.01$, $\rho = 10$, and, $\gamma = 0.9$. We arbitrarily set $\alpha' = 0.05$ at depths shallower than $z' = -2$ and linearly increase α' to 0.25 at $z' \leq -3$ (Fig. 7a). We use a rather low α' in order to accentuate the variation of interseismic creep. In laboratory studies of granite under hydrothermal conditions, $a \approx 0.015$ in the upper crust (Blanpied *et al.* 1991), and for $\mu = 30$ GPa, $D = 10$ km, and $s_o = 10$ m, $\alpha' = 0.05$ corresponds to a effective normal traction across the fault of about 10 MPa. We also specify that α' increases by a factor of five at depth, which limits the spatial extent of post-seismic creep. The effects of the depth of the lower boundary are qualitatively the same for other fault rheologies.

When the lower boundary is sufficiently deep, the mature interseismic creep rates adjacent to the asperity are initially high, and then decrease through the interseismic period (Fig. 7c). The depressed creep rates later in the interseismic period lead to a region of the fault larger than the asperity that may appear locked. When the lower boundary is close below the asperity, the transient post-seismic creep occurs over a shorter period compared to when the lower boundary is deeper, and the mature interseismic creep rates increase during the later interseismic period (Fig. 7b). This later increase in interseismic creep rates is greatest in the deep portions of the fault, although it is also apparent at shallow depths above the asperity, and is due to the proximity of the imposed steady creep below $z' = -3$. When the lower boundary is at $z' = -6$, transient

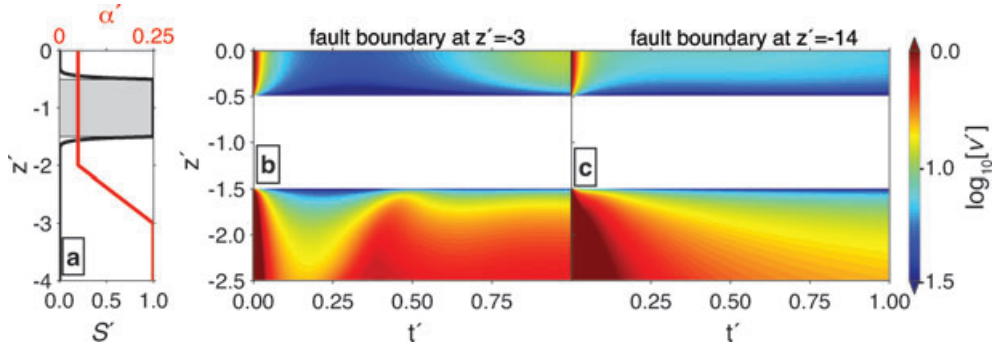

Figure 7. (a) Coseismic slip (black) and α' (red) in a 2-D vertical strike-slip fault model with an RS friction fault ($\rho = 10$, $L' = 0.01$, $\gamma = 0.9$); shaded area is the locked portion of the fault. (b) and (c) Mature interseismic creep rate in a model with a lower fault boundary at $z' = -3$ (b) or $z' = -14$ (c).

© 2010 The Authors, *GJI*, **181,** 81–98
Journal compilation © 2010 RAS

interseismic creep is only slightly affected by the fault loading, and when $z' = -10$ there is no effect on the transient creep near the asperity.

4 INTERSEISMIC CREEP AND FAULT RHEOLOGY

In this section, we further explore the dependence of interseismic creep on the parameters of the fault rheology. We continue to use 2-D models of an infinitely long, strike-slip fault, as described in Section 3.1 (Fig. 3). In the unlocked region of the fault, we consider linear viscous, non-linear viscous, RD friction, and RS friction faults, and we assume that the rheology is constant with depth. As our primary interest in this study is the velocity strengthening regime, we explore interseismic creep only for velocity strengthening frictional fault rheology parameters ($a - b > 0$ or equivalently $\gamma < 1$). We only consider spun-up models, assuming periodic earthquakes. We compare creep in models with RS friction faults to creep in a model with an RD friction fault in Section 4.4, but we do not directly compare models of other fault rheologies.

4.1 Linear and non-linear viscous fault zones

Fig. 8 shows cycle invariant interseismic creep in models with linear ($n = 1$) and non-linear ($n = 3$) viscous fault rheologies. When $n > 1$, heightened post-seismic creep rates are more localized near the asperity than when $n = 1$, due to an effective weakening of the non-linear viscous fault resulting from large traction near the asperity. As α_n' increases, there is less post-seismic creep, and more of the fault creeps steadily at the fault loading rate during the entire interseismic period. The average traction on a mature viscous fault is $\alpha_n'^{1/n}$ (i.e. the traction required to creep steadily at v_T), and as α_n' increases, coseismic traction changes are smaller relative to the background traction. For decreasing α_n' there is more pronounced transient creep following an earthquake, with depressed creep rates in the later seismic cycle. Analogous to the inverse of the Savage parameter, α_n' is effectively the relaxation time of the fault relative to the recurrence times of the earthquakes (Savage & Prescott 1978; Hetland & Hager 2006b; DiCaprio *et al.* 2008).

4.2 Rate-dependent friction fault zones

We show cycle invariant interseismic creep in models with RD friction fault rheologies in Fig. 9. As α_h' decreases, post-seismic transient creep extends over a larger region of the fault and propagates from the asperity at a higher rate. Because $\alpha_h' = (a - b)\sigma_E'$, a decrease in α_h' can reflect a decrease in σ_E', and one would indeed expect more transient post-seismic creep as the fault becomes less clamped. As α_h' increases, the fault creeps steadily at the fault loading rate over more of the fault. Increasing ρ_h results in slightly less initial transient creep, although the creep is weakly dependent on variations of ρ_h, especially compared to variations in α_h'. Because only changes in α_h significantly affect the degree that creep varies through the interseismic period, we might conclude that α_h' largely controls the apparent strength of the fault, although the average traction on the fault over multiple seismic cycles is $\alpha_h'\rho_h$. Roughly speaking, α_h' behaves for an RD friction fault as α_n' does for a viscous fault, although we note that α_n' depends on the recurrence time, T, whereas α_h' is independent of T.

4.3 Rate-state friction faults

We show the dependence of cycle invariant creep on RS frictional parameters in Fig. 10. As with α_h' in an RD friction model, decreasing α' results in broader regions of post-seismic creep and a larger variation in creep rates throughout the interseismic period. Similar to ρ_h in an RD friction model the parameter ρ has only a minor effect on the variation of creep through the interseismic period. Decreasing γ results in less transient creep farther from the asperity, and $\gamma \to 1$ results in sharper onset of post-seismic creep at depth (Fig. 11). Decreasing L' in an RS friction model results in more transient post-seismic creep, as well as a sharper onset of creep farther from the asperity (Fig. 10).

Far from the asperity, the fault creeps steadily at the fault loading rate, and $\Omega \approx 1$ during the entire interseismic period. Generally, $\Omega > 1$ prior to the onset of the post-seismic creep, while except for large L', $\Omega \approx 1$ during most of the later post-seismic and interseismic periods (Figs 10). $\Omega \approx 1$ signifies that fault creeps at steady state (i.e. $v' = L'/\theta'$), while for $\Omega > 1$ ($\Omega < 1$) the fault creeps faster (slower) than steady state. When $L' \leq 10^{-2}$, transient post-seismic creep is

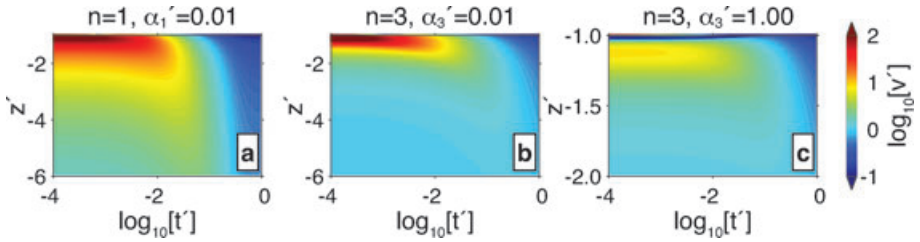

Figure 8. Mature interseismic fault creep in 2-D models (Fig. 3) with linear ($n = 1$) or non-linear ($n = 3$) viscous rheologies. Note the change in z' range in (c).

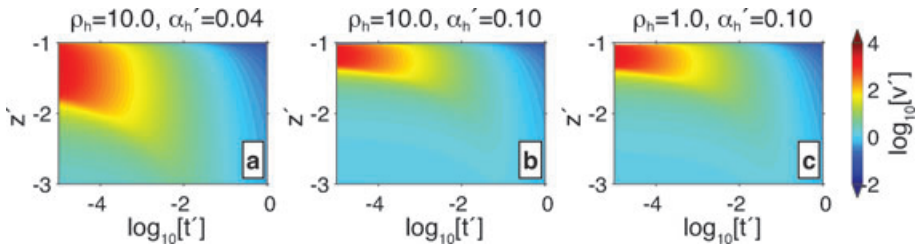

Figure 9. Mature interseismic fault creep in 2-D models (Fig. 3) with RD friction rheologies.

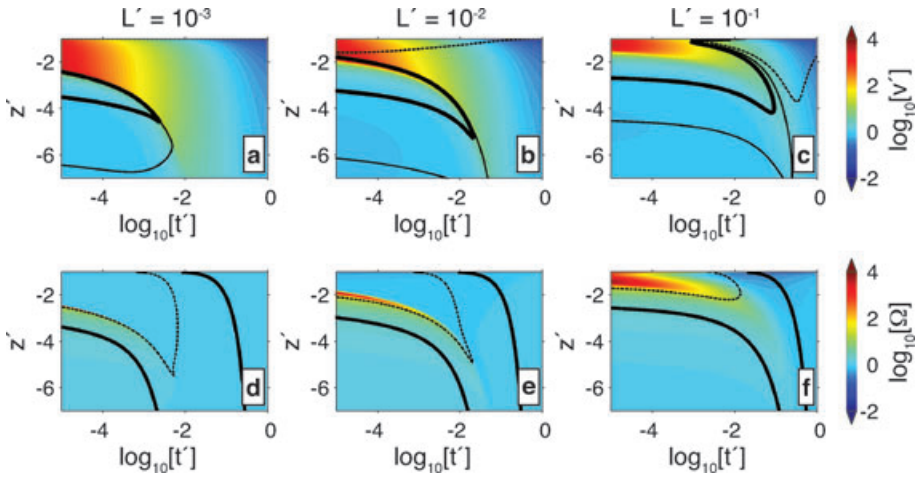

Figure 10. (a)–(c) Mature interseismic fault creep in 2-D models (Fig. 3) with RS friction rheologies ($\alpha' = 0.1$, $\gamma = 0.9$, and $\rho = 10$). Black lines represent the $\Omega = 0.8$ (dashed), 1.2 (thin solid), and 2.0-(thick solid) contours. (d)–(f) Ω corresponding to models in upper panels: black lines represent the $v' = 1$ (thick) and $v' = 10$ (dashed) creep rate contours.

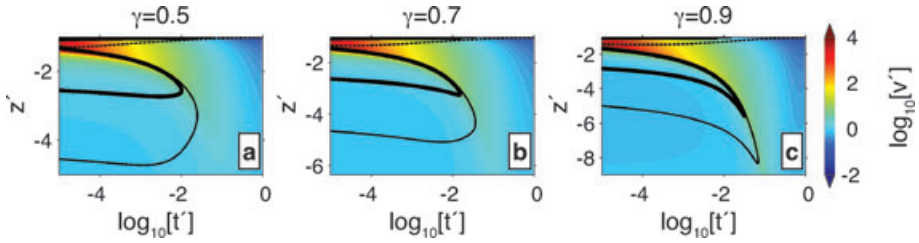

Figure 11. Mature interseismic fault creep in 2-D models (Fig. 3) with RS friction rheologies ($\rho = 10$, $\alpha' = 0.10$, $L' = 0.01$). Black lines represent the $\Omega = 0.8$ (dashed), 1.2 (thin solid) and 2.0 (thick solid) contours.

activated over a relatively large region near the asperity (Fig. 10). As the coseismic stresses diffuse from the asperity, both creep rates and Ω increase. For low L', the onset of post-seismic creep away from the asperity is abrupt (i.e. a sharper creep front), and $\Omega \approx 1$ during the period of transient post-seismic creep (Fig. 10a). On the other hand, when $L' > 10^{-2}$, post-seismic creep is constrained near the asperity, while the onset of post-seismic creep farther away is more gentle, with $\Omega \gg 1$ during most of the period with heightened post-seismic creep (Fig. 10c). As γ decreases, the region over the fault in which $\Omega > 1$ is smaller (Fig. 11).

4.4 Comparison of RD and RS friction faults

When $\Omega = 1$, an RS friction model reduces to an RD friction model, with $\alpha'_h = \alpha'(1 - \gamma)$ and $\rho_h = \rho/(1 - \gamma)$. With these parameters, RD and RS friction models have identical steady states. In models with RS friction faults and low L', $\Omega \approx 1$ except during the onset of post-seismic creep. Hence, during the later interseismic period, the creep rates in RS models approach those in models with RD frictional faults, assuming that the two models have identical steady states (Fig. 12). However, the creep during the earliest interseismic period is still quite distinct in models with RD and RS friction faults, even with small L'. With RS frictional faults, the immediate post-seismic creep rates away from the asperity remain relatively low because the perturbation to traction due to coseismic slip is small in these regions (Figs 10 and 12b). Eventually as the perturbation to fault traction diffuses away from the asperity, both Ω and the post-seismic creep-rates increase, followed by an abrupt decrease of Ω towards steady-state, and a near-exponential decrease in the creep rates (Fig. 12b). As the post-seismic creep rates decay, $\Omega \to 1$, and the creep is similar to that in models with an RD friction fault. As L' decreases, the onset of post-seismic creep at depth becomes more abrupt. The sharp onset of post-seismic creep away from the asperities and the subsequent similarity to creep in RD friction models is the same as in the models discussed by Perfettini & Ampuero (2008).

5 DISCUSSION

We discuss our model formulation in the context of elastodynamic models that solve for both coseismic slip and interseismic creep. We also compare our formulation to previously proposed models of only post-seismic creep. We then discuss the traction level on a spun-up fault, RS versus RD friction rheologies, and transient creep in the context of our model. Finally, we briefly explore limitations of our model due to the lack of consistent coseismic variation of frictional state in RS frictional models, and our assumed mechanism of fault loading.

5.1 Comparison to earthquake models

In the model formulation we propose, we do not solve for coseismic slip, but interseismic creep is consistent with the imposed coseismic slip history and the fault rheology outside of the asperities. One can imagine that spontaneous earthquakes in models of the entire earthquake cycle would be similar to those applied in a particular instance of our model, given some heterogeneous velocity weakening rheology. Our main intended use of these models is to investigate the mechanical response of faults to given spatio-temporal

© 2010 The Authors, *GJI*, **181,** 81–98
Journal compilation © 2010 RAS

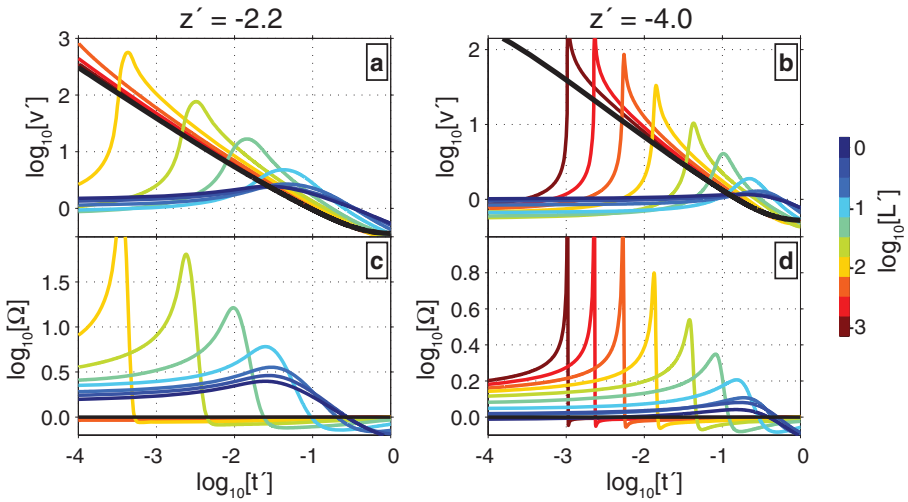

Figure 12. (a)–(b) Cycle invariant creep rates in models (Fig. 3) with an RD friction fault (black line; $\rho_h = 100$ and $\alpha'_h = 0.01$), and RS friction faults (solid coloured lines; $\rho = 10$, $\alpha' = 0.1$, $\gamma = 0.9$, and L' given in colour-scale) at $z' = -2.2$ (a) and -4.0 (b). (c–d) Ω in the RS friction (coloured lines) and RD friction (black line, $\Omega = 1$) fault models, corresponding to (a) and (b). Because $\alpha'_h = \alpha'(1-\gamma)$ and $\rho_h = \rho/(1-\gamma)$, friction in these models have identical steady states.

distributions of earthquakes, and to infer the mechanical properties of fault zones from geodetic observations without having to simultaneously search for permissible velocity weakening rheologies within asperities. Admittedly, there is some circularity in this strategy, as coseismic slip in the transition regions depends on the heterogeneous friction properties in both velocity weakening and strengthening regions (e.g. Boatwright & Cocco 1996; Tinti *et al.* 2005; Hillers & Wesnousky 2008), and thus inferred rheologies in transition regions may not be consistent with imposed coseismic slip. However, except for transition regions that are comparable in size to the asperity, the majority of the fault creep occurs outside of the transition regions. When there is significant coseismic slip in transition regions that are comparable to the size of the asperity, an elastodynamic model may be more appropriate to explore the post-seismic creep in the transition regions (see also Section 5.6).

The fundamental advantage of our model formulation over elastodynamic models of the full earthquake cycle, is the ability to pin calculations to particular asperity geometries and earthquake histories. In addition, because we do not solve for coseismic slip, our model is orders of magnitude faster to compute than the more complete elastodynamic models. The 2-D models we present here all took just minutes to spin-up on a desktop computer when we initially pre-stress the fault at τ_{steady}, and 3-D models presented in Paper 2, all took less than one hour to spin-up on a desktop computer. The 3-D model of Liu & Rice (2005) required about one day on a moderate computer cluster to integrate through one earthquake. The computational demand of calculating the coseismic slip limits the number of model permutations that can be considered. For instance, Kato (2008) explored over 100 different heterogeneous fault rheologies, and found at least one that qualitatively produced a similar earthquake sequence to the recent earthquakes in northeastern Japan. However, the timing of the modelled earthquakes was not the same as the observed, and thus it would not be possible to incorporate geodetic observations into the model success criteria. Nevertheless, this model demonstrated the strong feedback between interseismic creep and earthquakes, and thus the importance of modelling the full seismic cycle. In particular, Kato (2008) noted that the non-linearity of these frictional models make it exceedingly difficult to find a fault rheology, including both asperity and non-asperity regions, that will be consistent with all data. Due to the relatively low computation cost of our model formulation, a wide range of asperity geometries, coseismic slip histories and fault rheologies can be explored.

Finally, in fully elastodynamic earthquake cycle models, the size of the fault is limited to only slightly larger than the size of the asperities (e.g. Liu & Rice 2005; Hori 2006; Kato 2008). The need to limit the fault size is driven by the computational demands of calculating the evolution of coseismic slip. In Section 3.3, we showed that limited fault size can greatly influence the calculation of interseismic creep, especially late in the seismic cycle. If geodetic observations of interseismic deformation are to be used to infer rheologies, the fault domain should be much larger than the asperities in order to ensure that the calculated interseismic creep behaviour is not adversely affected by the prescribed fault loading (i.e. the boundary conditions).

5.2 Comparison to post-seismic fault creep models

There have been several studies that have described geodetic observations of post-seismic deformation using models with localized creep on frictional faults. Among these are the models of Hearn *et al.* (2002, 2009), Johnson *et al.* (2006), Perfettini & Avouac (2007), and Barbot *et al.* (2009). Hearn *et al.* (2002, 2009), Perfettini & Avouac (2007) and Barbot *et al.* (2009) used an RD friction fault rheology, while Johnson *et al.* (2006) used an RS friction fault rheology. The models of Hearn *et al.* (2002, 2009) were based on finite element calculations, but the models of Johnson *et al.* (2006) and Perfettini & Avouac (2007) used essentially the same formulation as we present here. The two key differences between our methodology and the previous studies, are that those models were not spun-up, and they used different criteria for where post-seismic fault creep was allowed to occur. We also consider a wider range of plausible fault rheologies.

Investigating the post-seismic deformation following the 2005 Parkfield earthquake, Johnson *et al.* (2006) assumed that the initial pre-earthquake fault traction, τ_{pre}, depended on the pre-earthquake fault creep rates, v_{pre}. Using spring-and-slider models, Johnson *et al.* (2006) found that τ_{pre} could be approximated by RD friction for

certain frictional parameters, particularly for small L (referred to as D_c in their paper). We refer to the RD friction approximation of $\tau_{\rm pre}$ as

$$\tau'_{\rm RD} = \alpha'_h(\log\{v'_{\rm pre}\} + \rho_h). \tag{20}$$

For $v_{\rm pre}$, Johnson *et al.* (2006) used the interseismic creep rates on the Parkfield segment of the San Andreas fault inferred by Murray *et al.* (2001). These interseismic creep rates were determined by the inversion of steady geodetic data recorded over several years prior to the Parkfield earthquake (Murray *et al.* 2001). In our models with RS frictional faults, $\tau'_{\rm RD}$ calculated using the creep rates immediately prior to a mature earthquake is not identical to the actual fault traction prior to that earthquake. This difference is largely due to the finite value of L' often assumed in these calculations. As $L' \to 0$, $\tau'_{\rm pre}$ in our spun-up models approaches $\tau'_{\rm RD}$, and for $L' \approx 10^{-2}$, the difference between $\tau'_{\rm pre}$ and $\tau'_{\rm RD}$ is negligible compared to the coseismic change in traction, making this particular difference with the model of Johnson *et al.* (2006) relatively insignificant. In a model of post-seismic deformation following the 1992 Landers earthquake, Perfettini & Avouac (2007) also effectively assumed that the pre-earthquake fault traction was that given by eq. (20). However, they simultaneously solved for a homogeneous $v_{\rm pre}$ and the post-seismic fault creep from the geodetic observations. Assuming that $v_{\rm pre}$ is consistent with the long-term earthquake history of the fault, both approximations of Johnson *et al.* (2006) and Perfettini & Avouac (2007) are reasonable. However, if $v_{\rm pre}$ is not well constrained, it is important to investigate the sensitivities of the model results to the pre-earthquake creep rates, or equivalently the pre-earthquake traction. Using our model formulation, observations of both the interseismic deformation prior to an earthquake and the post-seismic deformation could be used to constrain a spatially variable $v_{\rm pre}$ and post-seismic creep using a consistent model.

The more crucial difference between our formulation and those of Johnson *et al.* (2006) and Perfettini & Avouac (2007) is the assumption of where post-seismic creep is allowed to occur. Johnson *et al.* (2006) only solved for post-seismic creep where the coseismic traction change is positive (i.e. leading to post-seismic creep in the same direction of the imposed coseismic slip). Similarly, Perfettini & Avouac (2007) only calculated post-seismic creep below the inferred brittle–ductile transition at 15 km depth, and the coseismic perturbation to fault traction at these depths was positive. The authors implicitly assumed that any coseismic slip deficit in the regions where they did not allow post-seismic creep would be filled in either by future earthquakes or creep later in the interseismic period. However, even if these regions do not creep immediately following the earthquake, by not calculating the creep in some regions of the fault that may post-seismically creep, the relaxation of coseismic stresses may be impaired, and as a result the predicted post-seismic creep in other regions may be biased.

To illustrate that artificially locking non-asperity regions of the fault may interfere with post-seismic creep, we consider model 4 in Section 3.2 (Fig. 6). The coseismic slip in model 4 tapers to zero over a fairly broad region of the fault (Fig. 6a), and as a result, the coseismic traction change is negative over a broad region near the asperity (Fig. 6b). We assume that the initial fault traction is that from the fully spun-up model 4 shown in Fig. 6, and we calculate post-seismic creep making different assumptions on where creep is allowed. In the first model, post-seismic creep is allowed on the entire fault outside the asperity regardless of the sign of τ' ($z'_{\rm lock} > -1.0$ are the locked portions of the fault). The second model is equivalent to allowing post-seismic creep only where the coseismic traction change is positive ($z'_{\rm lock} > -1.2$), and this post-seismic locking criterion is as in Johnson *et al.* (2006). The third model allows post-seismic creep only where there is negligible coseismic slip ($z'_{\rm lock} > -1.5$), roughly equivalent to the assumption made by Perfettini & Avouac (2007).

Whether coseismic slip leads to negative fault traction depends on both the coseismic traction change and $\tau'_{\rm pre}$. In model 4, the time average traction through the interseismic period is $\tau'_{\rm steady} = \alpha'\rho = 0.5$, and coseismic slip does indeed lead to negative traction near the asperity (Fig. 13a). However, the traction becomes positive shortly after the earthquake, and there is negligible negative post-seismic creep where the traction is negative (Fig. 13b). For larger $\tau'_{\rm steady}$, for instance with $\rho = 100$, the traction may never be negative anywhere on the fault. Even in the model where post-seismic creep is permitted on the entire non-asperity region of the fault, there is negligible post-seismic creep immediately following the earthquake where traction is negative (Fig. 13b). (In this model, the post-seismic creep is at most 2.5×10^{-3} in the opposite direction to coseismic slip.) Hence with this fault rheology, assuming that the fault does not post-seismically creep close to the asperity may be sufficient for $t' < 0.1$ following an earthquake. However, farther from the asperity fault creep in a fully consistent model is significantly different from the creep in the model where creep is only allowed in the region of positive coseismic traction change ($z'_{\rm lock} > -1.2$), especially in later times (Fig. 13b). When creep is only allowed on the part of the

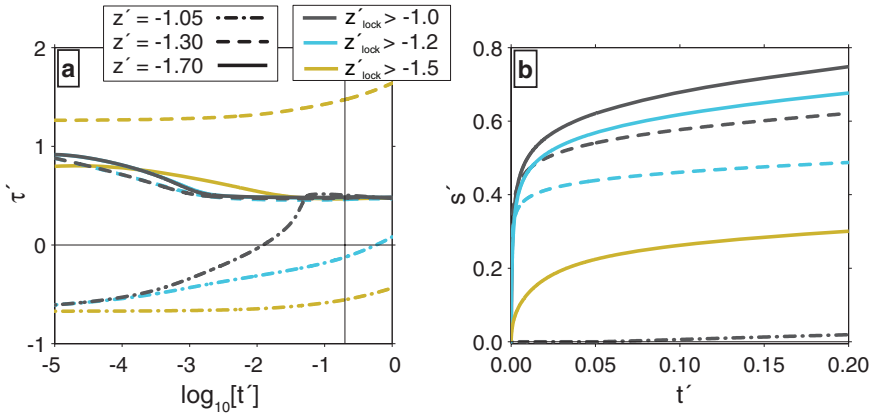

Figure 13. (a) Interseismic fault traction for three spun-up models, where the fault is locked at depths, $z'_{\rm lock}$, above -1.0 (black lines), -1.2 (cyan lines), or -1.5 (yellow lines). Traction is shown at three depths, as indicated in the legend. (b) Interseismic fault creep in the three models; line style is as in (a), and creep is only shown where it is allowed.

© 2010 The Authors, *GJI*, **181,** 81–98
Journal compilation © 2010 RAS

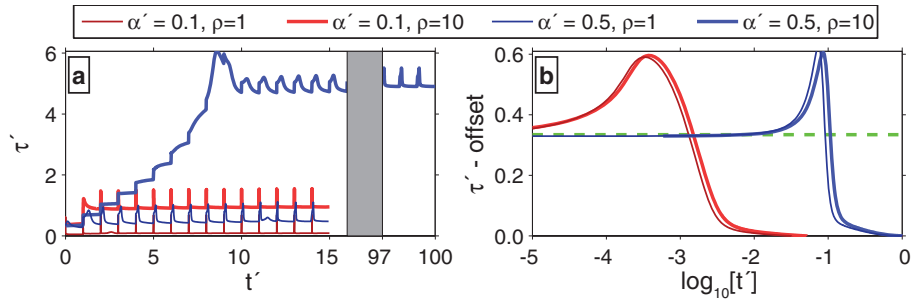

Figure 14. (a) Strike-slip fault traction at $z' = -1.5$ in model 4 of Fig. 6(a) with an RS fault rheology ($L' = 0.05$, $\gamma = 0.9$, and α' and ρ as indicated). (b) Cycle invariant fault traction at $z' = -1.5$, where time is relative to the start of a mature cycle, and traction is arbitrarily offset such that the $\tau' = 0$ at the end of the cycle. Green dashed line is the coseismic change in traction.

fault with no coseismic slip ($z'_{\rm lock} > -1.5$), there is an even greater disparity in post-seismic creep compared to the model in which we allow post-seismic creep in all non-asperity regions. Due to the strong dependence of the predicted creep on assumptions of where post-seismic creep is allowed, it is important to use fully spun-up models in which fault creep constraints are internally consistent with the long-term evolution of the fault. This consistency is especially critical when constraining fault rheologies from geodetic data.

5.3 Fault traction

In spun-up models with linear viscous fault rheologies, the average traction supported on faults over multiple seismic cycles is given by α'_1, while the degree that fault creep varies through the interseismic period is given by the inverse of α'_1. Hence, if rapid transient post-seismic fault creep was observed, one could conclude that the fault was weak surrounding the asperities. Fault strength and the degree of variation of interseismic creep are similarly related in models with non-linear viscous faults (Montési 2004b). In contrast to viscous faults, in models with frictional faults there is not necessarily any connection between the strength of a fault and the variation of interseismic creep rates. For instance, in Fig. 14 we show the effect of variations in RS frictional parameters on fault traction during spin-up of the model shown in Fig. 3. During spin-up, the traction increases from the initial traction (here assumed to be zero) to a traction that varies about $\rho\alpha'$ (Fig. 14a). Once spun up, the fault traction varies throughout the interseismic period, but the degree of variation is relatively insensitive to ρ and largely only dependent on α' (Fig. 14b). This behaviour is similar for RD frictional faults, where the average traction on a mature fault is $\rho_h\alpha'_h$, and α'_h has the largest effect on the degree of variation of creep during the interseismic period.

5.4 Rate-state and RD friction

As L' decreases, interseismic creep in models with RS frictional faults is similar to creep predicted in models assuming RD friction, although the creep following the earthquake is quite distinct (Fig. 12). Perfettini & Avouac (2007) and Perfettini & Ampuero (2008) have shown that creep in spring-and-slider models, with either velocity strengthening RS or RD friction, are identical except during early times. Similarly, Johnson *et al.* (2006) showed that spring-and-slider models with RS or RD friction are identical for certain frictional parameters, including low L. Perfettini & Ampuero (2008) investigated isolated perturbations to traction on a 2-D fault, and showed that RS and RD friction predict the same fault deformation as long as the spatial size of the traction perturbation is much larger than a critical distance $L_b = \frac{\mu L}{b\sigma_E}$. Signifying the spatial size of the stress perturbation with L_τ, and non-dimensionalizing both L_b and L_τ by D, $\gamma\alpha' L'_\tau \gg L'$ is required for RS and RD friction to be the same. In the models in Fig. 12, $\gamma = 0.8$, $\alpha' = 0.1$, and because coseismic slip perturbs the traction over $L'_\tau \approx 1/4$, RS friction reduces to RD friction only when $L' \ll 0.02$. In Fig. 12 when $L' > 10^{-2}$, the fault creep in the two frictional models are not the same during most of the interseismic, while for lower L' the two rheological models predict similar interseismic creep later in the seismic cycle.

For values of L' that may be reasonable for natural faults (e.g. Marone 1998a; Marone & Kilgore 1993; Lapusta & Rice 2003), RS and RD friction may predict similar deformation during most of the later interseismic period. However, the spatio-temporal pattern of post-seismic creep in models with RD friction or RS friction is quite distinct. For example, if post-seismic creep rates simply decay over a large region of the fault, the fault might be best described with RD friction or a viscous rheology. On the other hand, if post-seismic creep is resolved as a propagating creep pulse (i.e. post-seismic creep rate increases with time at a distance from the asperity), we would expect that the fault was best described with RS rheology. If the spatio-temporal details of the earliest post-seismic creep can not be resolved with geodetic observations, concluding that the fault rheology is viscous or RD frictional may be premature, because a velocity strengthening RS frictional fault with a sufficiently low L' may be permissible. For distinct creep pulses, the timescale over which creep rates increase will constrain L' (Perfettini & Ampuero 2008), as also shown in the spring-and-slider models of Fukuda *et al.* (2009).

5.5 Transient creep

It is important to note that in the models we show here, the transient post-seismic creep away from the asperity is qualitatively different than the unstable transient slip observed in the models of Perfettini & Ampuero (2008) or Helmstetter & Shaw (2009). In the models of Perfettini & Ampuero (2008), following certain perturbations to fault traction on a 2-D fault plane, transient slip on velocity strengthening faults became unstable, with the maximum creep rates increasing as a creep pulse propagated from the stress perturbation. Similarly, in the spring-and-slider model of Helmstetter & Shaw (2009), with some velocity strengthening RS frictional parameters, transient creep does not simply decay but increases in what they refer to as slow (i.e. aseismic) earthquakes. In our models, the post-seismic creep rates far from the asperity are never larger than the maximum creep rates close to the asperity. Perfettini & Ampuero

(2008) found that only when $L'_\tau \gg L'_b$ does transient slip occur, where the maximum creep rates at a distance from the asperity are larger than the creep rates near the asperity. For $L' = 0.01$, $\gamma = 0.8$ and $\alpha' = 0.1$, and the spatial size of traction perturbations need to be larger than $L'_b = 0.13$ in order to generate a transient slip episode. The smoother coseismic slip profiles we explore often lead to perturbations in fault traction larger than L'_b; however, coseismic traction perturbations are generally smoother and lower amplitude than those considered by Perfettini & Ampuero (2008). On the other hand, when there are large discontinuities in coseismic slip, the resulting coseismic stress perturbations occur over a much smaller spatial scale (Fig. 6). Helmstetter & Shaw (2009) found that for transient slip to occur for velocity strengthening RS friction, the initial instantaneous friction had to be greater than some critical value. Their model demonstrates that when fault friction is too large, transient slip may be initially impeded, although the fault may dynamically weaken as the state variable evolves, eventually leading to transient slip. Following Perfettini & Ampuero (2008) and Helmstetter & Shaw (2009) the question remains, what are the classes of coseismic slip distributions and fault rheologies that generate unstable transient slip during the early interseismic period? We explore a limited class of models with unstable post-seismic creep in Paper 2.

5.6 Rheology of the transition regions

In all of the RS friction models presented above, the frictional state variable, θ', varies during the interseismic period, but in these models we do not prescribe any change in θ' when we apply coseismic slip. During seismic rupture, θ' can vary over many orders of magnitude (e.g. Ampuero & Rubin 2008), and when not calculating coseismic slip, the coseismic change in θ' can be found by directly integrating eq. (17) for a given coseismic slip rate variation. As a first-order test of including coseismic variations of θ' in these calculations, we instantaneously change θ' to the steady-state value at seismic rupture speeds, $\theta'_{\rm co} = L'/v'$, when we apply coseismic slip (e.g. Ampuero & Rubin 2008). Taking 1 m s^{-1} to be a typical seismic rupture speed (e.g. Heaton 1990), and assuming $v_T = 3\,{\rm m}/100\,{\rm yr}$, during coseismic slip, we change θ' to $\theta'_{\rm co} = L'/10^9$ everywhere there is significant coseismic slip (i.e. coseismic slip $> 10^{-2} s_o$). When $\theta' = \theta'_{\rm co}$ in the transition regions immediately after coseismic slip is imposed, the effective friction of the fault in these regions is very small. As a result, the initial creep rates will be significantly higher than if the coseismic change in θ' was ignored. However, these extremely rapid creep rates are isolated near the asperity and decay rapidly during the immediate post-seismic period. Similar to the extremely rapid creep rates due to artificially large discontinuities in coseismic slip (Section 3.2), these rapid creep rates effectively result in an adjustment to the imposed coseismic slip, and have minor effect of the interseismic creep during the later post-seismic and interseismic period. The effect of coseismic changes in θ' on the later creep rates strongly depends on the size of the transition region relative to the asperity (i.e. the distance over which coseismic slip tapers to zero). For instance, in the models using the coseismic slip in Fig. 3, there is only a small difference in the model results after about $t' \approx 10^{-6}$ following the coseismic slip. Specifically, Fig. 12 is virtually identical if we account for a coseismic change in θ'. For larger coseismic slip in larger transition regions, coseismic changes in θ' are more significant. For instance the coseismic slip in model 4 of Section 3.2 (Fig. 6a) tapers to zero over a region of the fault up to 50 per cent of the asperity size.

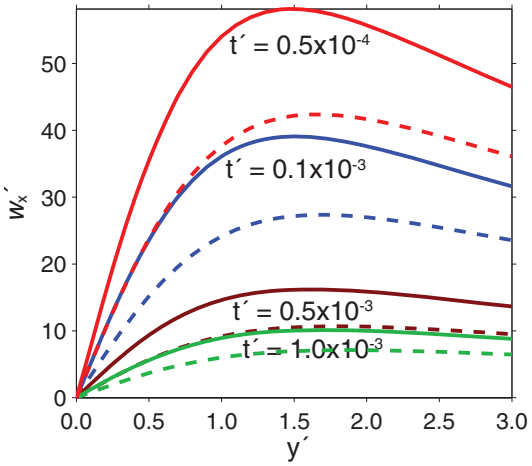

Figure 15. Cycle invariant fault parallel surface velocities in 2-D strike-slip models with coseismic slip as in model 4 of Fig. 6a, RS friction faults ($\gamma = 0.9$, $\rho = 10$, $L' = 0.05$ and $\alpha' = 0.05$), and θ' either remaining constant during coseismic slip (solid lines, same as in Fig. 6) or dropping to $\theta'_{\rm co}$ in regions of coseismic slip (dashed lines).

Accounting for a coseismic change in θ' affects the model results, with faster fault creep following the earthquake and a more rapid decay of the later post-seismic creep rates (Fig. 15).

5.7 Localized fault loading and distributed creep

In our model, we assume that the fault is loaded via back-slip, or equivalently imposed slip on the semi-infinite extension of the fault. This fault loading mechanism is the same as that considered in models that solve for both coseismic slip and interseismic creep (e.g. Rice 1993; Lapusta & Rice 2003; Liu & Rice 2005; Hillers & Wesnousky 2008; Perfettini & Ampuero 2008). Localized fault creep on continental faults transitions to distributed deformation at some depth below the seismogenic region. The deformation at depth, whether localized or distributed, is probably a response to both far-field fault loading and earthquake activity at seismogenic depths. Hence, it is unlikely that imposed steady creep at depth is a realistic boundary condition for continental faults. In Section 3.3, we demonstrated that by setting the bottom of the computational boundary sufficiently deep, the impact of the back-slip boundary condition on interseismic creep at shallow depths is minimized. For instance, when the lower fault boundary is only moderately deeper than the bottom of the seismogenic zone, the near surface fault creeps at a rate about 10 per cent of the fault loading rate later in the interseismic period (Fig. 7b). This behaviour is qualitatively similar to the 2-D strike-slip elastodynamic models where the bottom of the computational domain often lies at 25 km depth (e.g. Rice 1993; Lapusta & Rice 2003). Near-surface interseismic fault creep is not universally observed, although a coseismic slip deficit is often inferred at shallow depths (e.g. Simons *et al.*, 2002; Fialko *et al.* 2005). Our models indicate that when the effect of the back-slip boundary condition is sufficiently minimized, the near surface only creeps post-seismically, and does not creep appreciably in the later interseismic period. We note, however, that such post-seismic creep at shallow depths may not be consistent with observations from several continental earthquakes, where rapid shallow post-seismic slip was not observed (e.g. Fialko *et al.* 2005).

We ignore other processes that may affect not only the fault traction but also variations in effective normal stresses across the

fault. For instance, in fault systems, rarely is one fault isolated from other faults, and the stresses on one fault due to slip on nearby faults are not always negligible (e.g. Freed & Lin 2002; Hetland & Hager 2006b). Assuming linear elasticity, the stresses from other processes can be superimposed on our models, including models of strain accumulation on nearby faults. However, we emphasize that our formulation assumes that the stresses transfer entirely through elastic interactions. In subduction zones, stresses on the fault due to the deformation of the entire subducting slab and surrounding upper mantle flow may also be important (e.g. Conrad & Hager 1999; Kanda & Simons 2010). Inelastic bulk rheologies are also likely to be important, especially in the lower crust and upper mantle (e.g. Savage 1995; Wang 1995; Azúa *et al.* 2002; Freed & Bürgmann 2004; Fialko 2004; Johnson & Segall 2004; Freed *et al.* 2006; Hearn *et al.* 2009), where the inelastic component of stress transfer between faults may be significant (e.g. Li & Kisslinger 1984; Ruff 1996; Freed & Lin 2002). Linear bulk rheology can be included in this model formulation by including time dependence in the stress kernel and the surface displacement Greens functions, modifying eq. (1) to

$$\tau_i(\zeta, t) = \int_\Lambda \int_0^t s_j(\xi, \tau) K_{ji}(\zeta, t; \xi, \tau) \mathrm{d}\tau \, \mathrm{d}\xi. \tag{21}$$

By adopting time-dependent K and G, the influence of time-dependent bulk rheologies can be explored with these models. Eq. (21) only accounts for linear bulk rheologies, and if the non-linearity of rheologies is important over these time scales (e.g. Li & Kisslinger 1984), one would have to rely on other numerical techniques than those described here.

6 CONCLUSIONS

We describe a model of interseismic deformation due to fault creep. We consider linear viscous, non-linear viscous, RD friction, and RS friction fault rheologies. We assume that the fault is loaded by the extensions of the fault sliding steadily (equivalent to back-slip), and we assume that the bulk rheology is entirely elastic. We do not attempt to solve for earthquakes, rather we impose the geometries and histories of coseismic slip, and only solve for aseismic creep. The creep includes both transient post-seismic creep and near-steady creep during the later interseismic period, and results directly from coseismic slip and fault loading. The size of the computational domain is crucially important in these models, and the boundaries of the fault should be sufficiently far from the region of interest, so that the stresses due to the loading do not dominate the solution. When the fault domain is only slightly larger than the asperities, close to the asperities the fault creeps near the fault loading rate throughout the later interseismic period. On the other hand, when the fault domain is much larger than the size of the asperities, creep rates near the asperities are initially high following an earthquake, and then decay such that late in the seismic cycle creep rates are relatively low surrounding the asperities.

We propose this model to explore aseismic fault creep during the seismic cycle, as well as to constrain fault rheologies from geodetic observations in cases where the coseismic slip history is known. Both post-seismic creep and patterns of low creep surrounding asperities depend on recent coseismic slip and fault rheologies, but are weakly dependent on the average traction on the fault over multiple seismic cycles. In models with viscous or frictional faults, elevated creep rates propagate from the coseismic slip as pulses of post-seismic creep. For a viscous or an RD frictional fault model, these post-seismic pulses are smooth and broad. On the other hand, in models with RS frictional faults, the post-seismic pulses tend to be more distinct, with pronounced creep fronts and elevated post-seismic creep rates lasting over a longer period compared to in models with RD friction. As L' decreases, the pulse of post-seismic creep propagates from the asperity at a faster rate and with a more rapid onset of transient creep; however, after the front of the post-seismic creep pulse has passed, the post-seismic creep is similar to in a model with an RD friction fault. Observations of either interseismic or post-seismic deformation can be used to test plausible fault rheologies. When only considering a short period of time, there are trade-offs between fault rheology and imposed coseismic slip. Observations over longer periods of time will reduce these trade-offs, and simultaneous modelling of interseismic and post-seismic geodetic observations would provide the strongest constraints on fault rheologies.

ACKNOWLEDGMENTS

We thank the editor, M. Cocco, and L. Montési, and J. Loveless for comments and suggestions. We gratefully acknowledge discussions with J.-P. Avouac, N. Lapusta, and R. Kanda. All calculations were done using Matlab, The Mathworks Inc. This research was supported in part by the Gordon and Betty Moore Foundation. This is Caltech Tectonic Observatory contribution #116 and Caltech Seismological Laboratory contribution #10,032.

REFERENCES

Aki, K., 1984. Asperities, barriers, characteristic earthquakes and strong motion prediction, *J. geophys. Res.,* **89,** 5867–5872.

Ampuero, J. & Rubin, A.M., 2008. Earthquake nucleation on rate and state faults—aging and slip laws, *J. geophys. Res.,* **113**(B1), doi:10.1029/2007JB005082.

Azúa, B., DeMets, C. & Masterlark, T., 2002. Strong interseismic coupling, fault afterslip, and viscoelastic flow before and after the Oct. 9, 1995 Colima-Jalisco earthquake: continuous GPS measurements from Colima, Mexico, *Geophys. Res. Lett.,* **29,** 1821, doi:10.1029/2002GL014702.

Barbot, S., Fialko, Y. & Bock, Y., 2009. Postseismic deformation due to the M_w 6.0 2004 Parkfield earthquake: Stress-driven creep on a fault with spatially variable rate-and-state friction parameters, *J. geophys. Res.,* **114,** B07405, doi:10.1029/2008JB005748.

Ben-Zion, Y. & Rice, J., 1995. Slip patterns and earthquake populations along different classes of faults in elastic solids, *J. geophys. Res.,* **100,** 12 959–12 983.

Bilek, S. & Lay, T., 2002. Tsunami earthquakes possibly widespread manifestations of frictional conditional stability, *Geophys. Res. Let.,* **29,** 1673, doi:10.1029/2002GL015215.

Blanpied, M., Lockner, D. & Byerlee, D., 1991. Fault stability at hydrothermal conditions, *Geophys. Res. Lett.,* **18,** 609–1612.

Boatwright, J. & Cocco, M., 1996. Frictional constraints on crustal faulting. *J. geophys. Res.,* **101,** 13 895–13 909.

Bürgmann, R., Kogan, M.G., Steblov, G.M., Hilley, G., Levin, V.E. & Apel, E., 2005. Interseismic coupling and asperity distribution along the Kamchatka subduction zone, *J. geophys. Res.,* **110,** B07405, doi:10.1029/2005LB003648.

Chlieh, M. *et al.*, 2007. Coseismic slip and afterslip of the great Mw 9.15 Sumatra-Andaman earthquake of 2004, *Bull. seism. Soc. Am.,* **97,** doi:10.1785/0120050631, S152–S173.

Conrad, C. & Hager, B., 1999. Effects of plate bending and fault strength at subduction zones on plate dynamics, *J. geophys. Res.,* **104,** 17 551–17 571.

DiCaprio, C., Simons, M., Kenner, S. & Williams, C., 2008. Post-seismic reloading and temporal clustering on a single fault, *Geophys. J. Int.,* **172,** doi:10.1111/j.1365-246X.2007.03622.x, 581–592.

Dieterich, J., 1979. Modeling rock friction I: experimental results and constitutive equations, *J. geophys. Res.,* **84,** 2161–2168.

Dormand, J., 1996. *Numerical Methods for Differential Equations: A Computational Approach,* pp. 368, CRC Press LLC, New York.

Fialko, Y., 2004. Evidence of fluid-filled upper crust from observations of postseismic deformation due to the 1992 Mw7.3 Landers earthquake, *J. geophys. Res.,* **109**(B8), doi:10.1029/2004JB002985.

Fialko, Y., Sandwell, D., Simons, M. & Rosen, P., 2005. Three dimensional deformation caused by the Bam, Iran, earthquake and the origin of shallow slip deficit, *Nature,* **435,** 295–299.

Freed, A.M., 2007. Afterslip (and only afterslip) following the 2004 Parkfield, California, earthquake, *Geophys. Res. Lett.,* **34,** 6, doi:10.1029/2006GL029155.

Freed, A. & Bürgmann, R., 2004. Evidence of power-law flow in the Mojave desert mantle, *Nature,* **430,** doi:10.1038/nature02784, 548–551.

Freed, A. & Lin, J., 2002. Accelerated stress buildup on the southern San Andreas fault and surrounding regions caused by Mojave Desert earthquakes, *Geology,* **30,** 571–574.

Freed, A.M., Bürgmann, R., Calais, E., Freymueller, J. & Hreinsdóttir, S., 2006. Implications of deformation following the 2002 Denali, Alaska, earthquake for postseismic relaxation processes and lithospheric rheology, *J. geophys. Res.,* **111,** B1, doi:10.1029/2005JB003894.

Fukuda, J., Johnson, K.M., Larson, K. & Miyazaki, S., 2009. Fault friction parameters inferred from the early stages of afterslip following the 2003 Tokachi-oki earthquake, *J. geophys. Res.,* **114,** B04412, doi:10.1029/2008JB006166.

Hearn, E., Bürgmann, R. & Reilinger, R., 2002. Dynamics of İzmit earthquake postseismic deformation and loading of the Düzce earthquake hypocenter, *Bull. seism. Soc. Am.,* **92,** 172–193.

Hearn, E., Ergintav, S., McClusky, S. & Reilinger, R., 2009. İzmit earthquake postseismic deformation and dynamics of the North Anatolian Fault Zone, *J. geophys. Res.,* **14,** B08405, doi:10.1029/2008JB006026.

Heaton, T., 1990. Evidence for and implications of self-healing pulses of slip in earthquake rupture, *Phys. Earth planet Int.,* **64,** 1–20.

Helmstetter, A. & Shaw, B., 2009. Afterslip and aftershocks in the rate-and-state friction law, *J. geophys. Res.,* **114,** B01308, doi:10.1029/2007JB005077.

Hetland, E. & Hager, B., 2005. Postseismic and interseismic displacements near a strike-slip fault: a two-dimensional theory for general linear viscoelastic rheologies, *J. geophys. Res.,* **110,** B10401, doi:10.1029/2005JB003689.

Hetland, E. & Hager, B., 2006a. The effects of rheological layering on postseismic deformation, *Geophys. J. Int.,* **166,** 277–292, doi:10.1111/j.1365-246X.2006.02974.x.

Hetland, E. & Hager, B., 2006b. Interseismic strain accumulation: spin-up, cycle invariance, and irregular rupture sequences, *Geochem. Geophys. Geosyst.,* **7,** Q05004, doi:10.1029/2005GC001087.

Hillers, G. & Wesnousky, S., 2008. Scaling relations of strike-slip earthquakes with different slip-rate-dependent properties at depth, *Bull. seism. Soc. Am.,* **98,** doi:10.1785/0120070200, 1085–1101.

Hori, T., 2006. Mechanisms of separation of rupture area and variation in time interval and size of great earthquakes along the Nankai Trough, southwest Japan, *J. Earth Sim.,* **5,** 8–19.

Hsu, Y. *et al.*, 2006. Frictional afterslip following the 2005 Nias-Simeulue earthquake, Sumatra, *Science,* **312,** doi:10.1029/2003JB002917, 1921–1926.

Johnson, K.M. & Segall, P., 2004. Viscoelastic earthquake cycle models with deep stress-driven creep along the San Andreas fault system, *J. geophys. Res.,* **109,** B10403, doi:10.1029/2004JB003096.

Johnson, K.M., Bürgmann, R. & Larson, K., 2006. Frictional properties on the San Andreas Fault near Parkfield, California, inferred from models of afterslip following the 2004 earthquake, *Bull. seism. Soc. Am.,* **96,** doi:10.1785/0120050808, S321–S338.

Jónsson, S., Segall, P., Pedersen, R. & Bjornsson, G., 2003. Post-earthquake ground movements correlated to pore-pressure transients, *Nature,* **424,** doi:10.1038/nature01776, 179–183.

Kanamori, H., 1986. Rupture process of subduction-zone earthquakes, *Ann. Rev. Earth planet. Sci.,* **14,** 293–322.

Kanda, R.V.S. & Simons, M., 2010. An elastic plate model for interseismic deformation in subduction zones, *J. geophys. Res.,* in press, doi:10.1029/2009JB006611.

Kato, N., 2008. Numerical simulation of recurrence of asperity rupture in the Sanriku region, northeastern Japan, *J. geophys. Res.,* **113,** B06302, doi:10.1029/2007JB005515.

King, G. & Wesnousky, S.G., 2007. Scaling of Fault Parameters for Continental Strike-Slip Earthquakes, *Bull. seism. Soc. Am.,* **97,** doi:10.1785/0120070048, 1833–1840.

Lapusta, N. & Rice, J., 2003. Nucleation and early seismic propagation of small and large events in a crustal earthquake model, *J. geophys. Res.,* **108,** 2205, doi:10.1029/2001JB000793.

Lapusta, N., Rice, J., Ben-Zion, Y. & Zheng, G., 2000. Elastodynamic analysis for slow tectonic loading with spontaneous rupture episodes on faults with rate- and state-dependent friction, *J. geophys. Res.,* **105,** 23 765–23 789.

Li, V.C. & Kisslinger, C., 1984. Stress transfer and nonlinear stress accumulation at subduction type plate boundaries—application to the Aleutians, *Pageoph,* **122,** 812–830.

Linker, M. & Rice, J., 1997. Models of postseismic deformation and stress transfer associated with the Loma Prieta earthquake, in *The Loma Prieta, California, Earthquake of October 17, 1989—Aftershocks and Postseismic Effects,* pp. 253–276, ed. Reasenberg, P.A., USGS Professional Paper 1550-D.

Liu, Y. & Rice, J., 2005. Aseismic slip transients emerge spontaneously in three-dimensional rate and state modeling of subduction earthquake sequences, *J. geophys. Res.,* **110,** B08307, doi:10.1029/2004JB003424.

Marone, C., 1998a. Laboratory-derived friction laws and their application to seismic faulting, *Annu. Rev. Earth planet. Sci.,* **26,** 643–696.

Marone, C., 1998b. The effect of loading rate on static friction and the rate of fault healing during the earthquake cycle, *Nature,* **391,** 69–72.

Marone, C. & Kilgore, B., 1993. Scaling of the critical slip distance for seismic faulting with shear strain in fault zones, *Nature,* **362,** 618–621.

Marone, C., Scholz, C. & Bilham, R., 1991. On the mechanics of earthquake afterslip, *J. geophys. Res.,* **96,** 8441–8452.

Matsu'ura, M. & Sato, T., 1989. A dislocation model for the earthquake cycle at convergent plate boundaries, *Geophys. J. Int.,* **96,** 23–32.

Meade, B., 2007. Algorithms for the calculation of exact displacements, strains, and stresses for triangular dislocation elements in a uniform elastic half space, *Comp. Geosci.,* **33,** doi:10.1016/j.cageo.2006.12.003, 1064–1075.

Miyazaki, S. & Heki, K., 2001. Crustal velocity field of southwest Japan: subduction and arc-arc collision, *J. geophys. Res.,* **106,** 4305–4326.

Miyazaki, S., Segall, P., Fukuda, J. & Kato, T., 2004. Space time distribution of afterslip following the 2003 Tokachi-oki earthquake: implications for variations in fault zone frictional properties, *Geophys. Res. Lett.,* **31,** L06623, doi:10.1029/2003GL019410.

Montési, L., 2004a. Controls of shear zone rheology and tectonic loading on postseismic creep, *J. geophys. Res.,* **109,** B10404, doi:10.1029/2003JB002925.

Montési, L.G.J., 2004b. Postseismic deformation and the strength of ductile shear zones, *Earth Planet Space,* **56,** 1135–1142.

Montési, L. & Hirth, G., 2003. Grain size evolution and the rheology of ductile shear zones: from laboratory experiments to postseismic creep, *Earth planet. Sci. Lett.,* **211,** doi:10.1016/S0012-821X(03)00196-1, 97–110.

Murray, J.R., Segall, P., Cervelli, P., Prescott, W. & Svarc, J., 2001. Inversion of GPS data or spatially variable slip-rate on the San Andreas Fault near Parkfield, CA, *Geophys. Res. Lett.,* **28,** 359–362.

Noda, H., Dunham, E. & Rice, J., 2009. Earthquake ruptures with thermal weakening and the operation of major faults at low overall stress levels, *J. geophys. Res.,* **114,** B07302, doi:10.1029/2008JB006143.

Norabuena, E. *et al.*, 2004. Geodetic and seismic constraints on some seismogenic zone process in Costa Rico, *J. geophys. Res.,* **109,** B11403, doi:10.1029/2003JB002931.

Ogawa, R. & Heki, K., 2007. Slow postseismic recovery of geoid depression formed by the 2004 Sumatra-Andaman Earthquake by mantle water diffusion, *Geophys. Res. Lett.,* **34,** L06313, doi:10.1029/2007GL029340.

Okada, Y., 1992. Internal deformation due to shear and tensile faults in a half-space, *Bull. seism. Soc. Am.,* **82,** 1018–1040.

Perfettini, H. & Ampuero, J., 2008. Dynamics of a velocity strengthening fault region: implications for slow earthquakes and postseismic slip, *J. geophys. Res.,* **113,** B09317, doi:10.1029/2007JB005398.

Perfettini, H. & Avouac, J., 2004. Postseismic relaxation driven by brittle creep: a possible mechanism to reconcile geodetic measurements and the decay rate of aftershocks, application to the Chi-Chi earthquake, Taiwan, *J. geophys. Res.,* **109,** B02304, doi:10.1029/2003JB002488.

Perfettini, H. & Avouac, J., 2007. Modeling afterslip and aftershocks following the 1992 Landers earthquake, *J. geophys. Res.,* **112,** B07409, doi:10.1029/2006JB004399.

Perfettini, H., Avouac, J. & Ruegg, J., 2005. Geodetic displacements and aftershocks following the 2001, *J. geophys. Res.,* **110,** B09404, doi:10.1029/2004JB003522.

Rice, J., 1993. Spatio-temporal complexity of slip on a fault, *J. geophys. Res.,* **98,** 9885–9907.

Rice, J. & Ben-Zion, Y., 1996. Slip complexity in earthquake fault models, *Proceed. Nat. Acad. Sci. USA,* **93,** 3811–3818.

Rice, J. & Gu, J., 1983. Earthquake aftereffects and triggered seismic phenomena, *Pure appl. Geophys.,* **121,** 187–219.

Rice, J., Lapusta, N. & Ranjith, K., 2001. Rate and state dependent friction and the stability of sliding between elastically deformable solids, *J. Mech. Phys. Solids,* **49,** 1865–1898.

Ruff, L., 1996. Large earthquakes in subduction zones: segment interaction and recurrence times, *in Subduction: Top to Bottom,* Vol. 96, pp. 91–104, eds Bebout, G.E., Scholl, D.W., Kirby, S.H. & Platt, J.P., AGU Geophysical Monograph.

Ruina, A., 1983. Slip instability and state variable friction laws, *J. geophys. Res.,* **88,** 10 359–10 370.

Savage, J., 1995. Interseismic uplift at the Nankai subduction zone, southwest Japan, 1951–1990, *J. geophys. Res.,* **100,** 6339–6350.

Savage, J.C. & Burford, R.O., 1973. Geodetic determination of relative plate motion in central California, *J. geophys. Res.,* **78,** 832–845.

Savage, J. & Prescott, W., 1978. Asthenosphere readjustment and the earthquake cycle, *J. geophys. Res.,* **83,** 3369–3376.

Savage, J., Svarc, J. & Yu, S., 2005. Postseismic relaxation and transient creep, *J. geophys. Res.,* **110,** B11402, doi:10.1029/2005JB003687.

Scholz, C.H., 1998. Earthquakes and friction laws, *Nature,* **391,** 37–42.

Simons, M., Fialko, Y. & Rivera, L., 2002. Coseismic deformation from the 1999 M-w 7.1 Hector Mine, California, earthquake as inferred from InSAR and GPS observations, *Bull. seism. Soc. Am.,* **92,** 1390–1402.

Suito, H. & Hirahara, K., 1999. Simulation of postseismic deformation caused by the 1896 Rikyu-u earthquake, northeast Japan: Re-evaluation of the viscosity in the upper mantle, *Geophys. Res. Lett.,* **26,** 2561–2564.

Suwa, Y., Miura, S., Hasegawa, A., Sato, T. & Tachibana, K., 2006. Interplate coupling beneath NE Japan inferred from three-dimensional displacement field, *J. geophys. Res.,* **111,** B04402, doi:10.1029/2004JB003203.

Thatcher, W. & Rundle, J., 1984. A viscoelastic coupling model for the cyclic deformation due to periodically repeated earthquakes at subduction zones, *J. geophys. Res.,* **89,** 7631–7640.

Tinti, E., Bizzarri, A. & Cocco, M., 2005. Modeling the dynamic rupture propagation on heterogeneous faults with rate- and state-dependent friction, *Ann. Gephys.,* **48,** 327–345.

Tinti, E., Cocco, M., Fukuyama, E. & Piatanesi, A., 2009. Dependence of slip weakening distance (Dc) on final slip during dynamic rupture of earthquakes, *Geophys. J. Int.,* **177,** doi:10.1111/j.1365-246X.2009.04143.x 1205–1220.

Wang, K., 1995. Coupling of tectonic loading and earthquake fault slip at subduction zones, *Pageoph,* **145,** 537–559.

Wang, K., 2007. Elastic and viscoelastic models of crustal deformation in subduction earthquake cycle, in *The Seismogenic Zone of Subduction Thrust Faults,* pp. 540–575, eds Dixon, T.H. & Moore, J.C., Columbia University Press, New York.

Wang, K. & He, J., 2008. Effects of frictional behavior and geometry of subduction fault on coseismic seafloor deformation, *Bull. seism. Soc. Am.,* **98,** doi:10.1785/0120070097, 571–579.

Wang, K., He, J., Dragert, H. & James, T., 2001. Three-dimensional viscoelastic interseismic deformation model for the Cascadia subduction zone, *Earth Planets Space,* **53,** 295–306.

Wang, K., Well, R., Mazzotti, S., Hyndman, R.D. & Sagiya, T., 2003. A revised dislocation model of interseismic deformation of the Cascadia subduction zone, *J. geophys. Res.,* **108,** 2026, doi:10.1029/2001JB001227.